ISSN 0128-7680

Pertanika Journal of Science & Technology

VOLUME NO. 33
ISSUE NO. 2
MAY- AUGUST 2025

ENRICHED PUBLICATIONS PVT. LTD

**S-9, IInd FLOOR, MLU POCKET,
MANISH ABHINAV PLAZA-II, ABOVE FEDERAL BANK,
PLOT NO-5, SECTOR-5, DWARKA, NEW DELHI, INDIA-110075,
PHONE: - + (91)-(11)-47026006**

ISSN 0128-7680

Pertanika Journal of Science & Technology

Aim & Scope

AIM

Pertanika Journal of Science & Technology is an official journal of Universiti Putra Malaysia. It is an open-access online scientific journal. It publishes original scientific outputs. It neither accepts nor commissions third party content.

Recognised internationally as the leading peer-reviewed interdisciplinary journal devoted to the publication of original papers, it serves as a forum for practical approaches to improve quality on issues pertaining to science and engineering and its related fields.

Pertanika Journal of Science and Technology is now published in English and it is open for submission by authors from all over the world. It is currently published 6 times a year, in January, March, April, July, August, and October.

ISSN 0128-7680

ISSN 0128-7680

ISSN 0128-7680

Pertanika Journal of Science & Technology

(Volume No. 33, Issue No. 2, May- August 2025)

Contents

No.	Articles/Authors Name	Pg. No.
1	Public Awareness and Performance Assessment of Communal Grease Traps in Klang Valley, Malaysia *-Theban Arumugam, Priyadarshini Ravindran, Shafreeza Sobri*, Salmiaton Ali and Mus'ab Abdul Razak*	1 - 19
2	Random Forest Model for Software Build Time Prediction on CI/ CD Pipeline *-Wen Han Seow1, Chia Yean Lim1* and Sau Loong Ang2*	20 - 37
3	A Novel Approach to Evaluating HEMA Polymer Gel Dosimeters Using Molecular Vibrational Features *- Muhammad Alhassan1,2*, Azhar Abdul Rahman1, Iskandar Shahrim Mustafa1, Mohd Zahri Abdul Aziz3, Mohd Zakir Kassim 3, Mohammed Salem Abdullah*	38 - 57
4	The Impact of Hydrocarbon R290 Refrigerant on Air Conditioner Performance and Environmental Sustainability *- Ferdinand Ng Siek Khai1,2 and Nurul Sabihah Zakaria1**	58 - 77

ISSN 0128-7680

Public Awareness and Performance Assessment of Communal Grease Traps in Klang Valley, Malaysia

Theban Arumugam, Priyadarshini Ravindran, Shafreeza Sobri*, Salmiaton Ali and Mus'ab Abdul Razak
Department of Chemical and Environmental Engineering, Faculty of Engineering, Universiti Putra Malaysia, 43400 UPM, Serdang, Selangor, Malaysia

ABSTRACT

The presence of fat, oil and grease (FOG) in wastewater has become an alarming concern and Malaysia is no exception. FOG that escapes into the sewer system can cause sewer network blockages and overflow, contamination of water bodies and inefficient sewerage treatment plant processes, which will harm the ecosystem. This paper aims to investigate the level of awareness and current practices on FOG management among food operators and management staff in selected hotels and shopping malls in Klang Valley, Malaysia. Analysis revealed that most respondents (81.2%) had perceived awareness of FOG, and 76.2% were aware of FOG management and practices on their premises. Although awareness levels for both management and operators are high, in reality, they have not been translated into practice. This is evident from investigating the effectiveness of the existing communal grease trap design by analyzing the effluent samples. The highest levels of biochemical oxygen demand (BOD) for hotel and shopping mall effluents were 9000 mg/L and 13000 mg/L, respectively, while chemical oxygen demand (COD) values in the effluent range from 30000 to 93000 mg/L. The oil and grease (O&G) and total suspended solids (TSS) values in the effluent were in the range of 50000-85000 mg/L and 10,000-72,000 mg/L, respectively. All tested parameters were well above the permissible limit based on Malaysia's Water Services Industry (Prohibited Effluent) Regulations 2021 (Regulation 4). This concludes that the communal grease traps investigated in this study are ineffective and most likely allow non-permissible effluent into the environment.

Keywords: *Awareness, communal grease trap, fat, oil and grease (FOG), management*

INTRODUCTION

Fat, oil, and grease (FOG) are harmful to the existing sewer network regardless of the origin of its source (Wallace et al., 2017). For this reason, legislation ensuring that effective FOG management is in place by food service operators is now being heavily enforced worldwide. In the Southeast Asian region, Thailand and Indonesia have emphasized the installation of grease traps for any food service establishment due to the potential of discharging significant amounts of FOG deposition in the sewer system. Malaysia, Brunei and Singapore have imposed strict regulations on installing grease traps to limit the discharge of FOG that is less than 50 to 100 mg/L into the sewer lines (Tang et al., 2024). In 2021, Malaysia introduced the Water Services Industry (Prohibited Effluent) Regulations 2021, which stipulated that no person is permitted to discharge any prohibited effluent, including discharges

of FOG that is less than 50 to 100 mg/L into the sewer lines (Tang et al., 2024). In 2021, Malaysia introduced the Water Services Industry (Prohibited Effluent) Regulations 2021, which stipulated that no person is permitted to discharge any prohibited effluent, including discharges containing pollutants such as oil and grease, to a public sewage system or treatment plant without the approval of the National Water Services Commission (SPAN). Table 1 shows the discharge limit specified under the Water Services Industry (Prohibited Effluent) Regulations 2021.

Table 1
Discharge limit specified under Water Services Industry (Prohibited Effluent) Regulations 2021

Item	Parameter	Unit	Limit
1.	Temperature	°C	40
2.	pH	-	6.0 – 9.0
3.	Biological Oxygen Demand (BOD)	mg/L	250
4.	Suspended Solids (SS)	mg/L	300
5.	Chemical Oxygen Demand (COD)	mg/L	500
6.	Total Nitrogen (TN)	mg/L	50
7.	Ammoniacal Nitrogen (AMN)	mg/L	30
8.	Total Phosphorus (TP)	mg/L	10
9.	Oil and Grease (O&G)	mg/L	50

A grease trap is the most common and economical solution to intercept the FOG and, therefore, reduces the amount that enters the main sewers, which can cause inconvenience to the authorities, contractors, end users and the public such as blocked sewer pipelines, overflowing manholes, and flooding of walkways, roads and public amenities (Nieuwenhuis et al., 2018). Grease traps work on the basic principle of gravity, where FOG floats on water and solid particles sink (Aziz, 2010). Baffles within the trap slow the inflow of wastewater from the kitchen sinks. This encourages a settlement period where the separation of fats, oils, grease, water and solid food particles occur within the unit. A trap on the inlet prevents FOG from flowing directly through the unit, with the FOG retained within the unit with food particles, allowing cleaner water to flow through. The retained waste will build up over time and requires regular service and removal of waste for disposal (Aziz et al., 2011).

Today, most pipelines from commercial kitchens, such as floor traps and pot wash areas that use dishwashing detergent, are connected to the sink wastewater pipeline carrying FOG. If the purity of the wastewater or effluent is questionable, the grease trap will be deemed unfit or ineffective (Chinwetkitvanich & Ektaku, 2020).

The fact that FOG is considered accountable for 50–70% of sewer blockages worldwide triggers questions about the claimed efficacy of grease traps in retaining 50%–90% of FOG (Sultana et al., 2022). The consultants usually determine the dimension of the grease trap during the design phase based on kitchen capacity and usage factors. The unprecedented pipeline modifications and unplanned increased usage contribute to the ineffectiveness of the grease trap, which is designed for a specific population or person equivalent. The uncontrolled flow of effluent more than often forces the FOG from the first chamber to the next and subsequently to the grease trap outlet, thus escaping the trap. This is often related to the unexpected increase in usage compared to the expected volume during the design phase. Over time, modifications to the pipeline due to additional sinks, cooking stations, and new pipelines have also contributed to the increased flow of FOG. In addition, the maintenance of grease traps by emptying, cleaning, and disposing of the collected FOG in a timely manner influences the grease traps' efficiency (He et al., 2017; Sultana et al., 2022). Current monitoring of the grease traps is done manually based on historical data with poor closed-loop inspection and improvements, thus resulting in overflows, spillages and, in some cases, blockages causing backflow (Wallace et al., 2017; Ali et al., 2022). The cost of clearance, the acute and complex treatment requirements, and the potential for environmental pollution and health risks during sewer overflows make this issue a concern.

Studies have shown that grease trap efficiency is influenced by volatile influent flow that impacts the hydraulic residence times and physical and chemical characteristics of the FOG, such as pH, chemical oxygen demand, dissolved oxygen, biological oxygen demand, total solids and depth of FOG layer. Understanding the physicochemical properties of the FOG, as well as the discharge characteristics, will help in the successful control of FOG deposition. Tang et al. (2024) conducted several site investigations at different food service establishments in Kuching, Sarawak. A significant difference in solid and dissolved constituents was discovered between the inlet and outlet chambers of the grease traps, indicating that the baffle wall could affect the separation mechanism. Ahmad et al. (2023) characterized the restaurant wastewater collected from a central grease interceptor situated at UTM Residensi, Kuala Lumpur. It was found that the COD, BOD and FOG values were 9948, 3170, and 1640 mg/l, respectively, well above the permitted discharge standards given by the Department of Environment, Malaysia.

On top of design standards, inspection and enforcement, one of the key elements in the FOG program is public awareness directed at reducing the amount of FOG discharged from food establishments and ensuring those handling the FOG waste are properly trained (Wallace et al., 2017). Ultimately, awareness among food establishment operators on the grease trap installation and maintenance determines the success or failure of FOG management. Collin et al. (2023) investigated the awareness of and experiences with FOG by those working within food service establishments. Findings demonstrate that awareness of issues caused by FOG in sewer networks is independent of job role or position and that

most respondents (74%) are acquainted with the impacts of poor FOG management.

Understanding the objectives of FOG management and its impact on the environment will help ensure that the waste is handled correctly from its origin until disposal. However, this is only viable when the standard operating procedures are governed by strict legislation to ensure compliance. In the United Kingdom, Water UK, in collaboration with several agencies, has established a guidance document to advise food establishments on the need to keep FOG out of drains and sewers (Water UK, 2017). Singapore's 2019 Code of Practice on Sewerage and Sanitary Works incorporates guidelines on the sizing of grease traps for all establishments that handle food, including restaurants, coffee shops and hawker centers (PUB, 2017). In Malaysia, the Ministry of Local Government Development has established a guideline stipulating the recommended design, installation, operation and maintenance of grease traps (KPKT, 2017). The existing law requires evidence of grease trap installation during business license applications or renewal with the local authorities. However, improvements must be made to the guidelines to include specific volumes and dimensions of the grease traps, as well as monitoring the cleaning schedule and frequency to avoid noncompliance.

This study investigated communal grease traps in 14 premises in Klang Valley, Malaysia, comprising hotels and shopping malls. Hotels have multiple kitchens working around the clock to cater to major events such as parties, weddings, company dinners, and room service. On the other hand, shopping malls have shared communal grease traps due to the high number of food and beverage eateries operating within the premises. Both hotels and shopping malls require significant manpower resources to ensure operations continue without disruption. Furthermore, they need to be properly trained to comply with standard operating procedures (SOP) to ensure standardization in food preparation, cleaning and waste management, particularly FOG.

While food service establishments are often assumed to be the major source of FOG deposits in the sewer, their contribution to the problem has not been thoroughly investigated. This research aims to (1) investigate the current practices and level of awareness of FOG management among food operators and management staff in selected hotels and shopping malls through questionnaire distribution and (2) quantify the discharge characteristics of the grease trap to assess the effectiveness of existing communal grease trap design. Samples were collected before and after passing through the grease traps and analyzed based on the following parameters: biochemical oxygen demand (BOD), chemical oxygen demand (COD), dissolved oxygen (DO), oil and grease (O&G), total suspended solids (TSS) and pH. The investigation was carried out to determine if these parameters comply with the permitted discharge standards given by the Department of Environment, Malaysia. The information gathered from this study

METHODOLOGY

Premises

The study focuses on 14 premises in Klang Valley, divided into two categories: shopping malls and hotels. Seven hotels and seven shopping malls were selected. For confidentiality reasons, the hotels and shopping malls are denoted as H and S, respectively. All the grease traps at the respective premises have relatively similar frequency in terms of usage, size and maintenance. Details related to hotel and restaurant operating information are described in Tables 2 and 3.

Table 2
Hotel operating information

Hotel	Number of kitchens	Kitchen cooking frequency	Hotel rating	Number of grease traps	Grease trap size (GPM)	Frequency of service (per month)
H1	6	Minimum 3 meals per day	5	8	500	4
H2	7		5	3	500	1
H3	5		5	2	500	8
H4	4		5	4	500	4
H5	3		4	2	500	4
H6	2		5	1	500	1
H7	1		3	1	500	2

Table 3
Shopping mall operating information

Shopping malls	Number of F&B	Kitchen cooking frequency	Number of grease traps	Grease trap size (GPM)	Frequency of service (per month)
S1	10	Continuously from 10 am to 9 pm	10	250	2
S2	30		6	250	4
S3	25		17	250	1
S4	5		2	250	1
S5	30		3	250	2
S6	56		21	250	2
S7	3		3	250	2

Instrument

The questionnaire was constructed based on expert consultation and an intensive literature review. Data collection was carried out by sharing questionnaires through Google Forms and face-to-face interviews with the respondents. The first section of the questionnaire included demography surveys on age, educational level, job categories, and premises location. The second section covered awareness

questions regarding FOG management. Current practices of FOG management at the premises were assessed in the third part of the instrument. Upon data collection, descriptive analysis in SPSS was used.

This survey used a nominal scale to gather the respondents' basic demographic information. The data required to understand awareness and practices were gathered using a 5-point Likert Scale ranging from (1) Strongly Disagree to (5) Strongly Agree. The questionnaire has gone through a process of validity and reliability testing. A pilot test was conducted to determine the questionnaire's reliability and ensure that the overall structure of the survey was in no way ambiguous. Cronbach's Alpha was found to be 0.84 and 0.81 for Sections 2 and 3, respectively. It is stated that a survey construct has a high level of reliability when the Alpha coefficient of the reliability test in the survey falls within the range of 0.7 and 0.9 (Straub et al., 2004).

Sampling

Wastewater samples were collected from the premises during the weekly maintenance the grease traps by a local service provider. Two samples were taken from each grease trap; influent samples were collected from the second chamber, where most of the FOG remained, while effluent samples were obtained from the final chamber before exiting into the sewer network. All samples were taken during the morning hours between 12:00 am and 3:00 am, and the sampling procedure was consistent throughout the study. The composite samples were collected using a 1-liter plastic bottle, a 500 mL plastic bottle preserved with sulphuric acid and a 1-liter glass bottle preserved with hydrochloric acid. Any foreign materials and rubbish found were discarded before samples were sent to an accredited lab to test for pH, biochemical oxygen demand (BOD), chemical oxygen demand (COD), dissolved oxygen (DO), oil and grease (O&G) and total suspended solids (TSS). Figure 1 summarizes the research activities involved in this work.

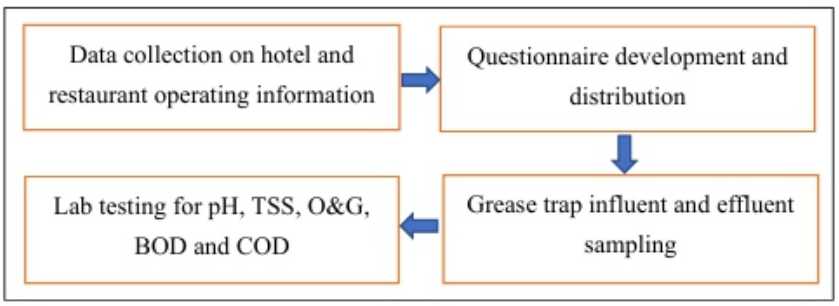

Figure 1. Flowchart of research activities

RESULT AND DISCUSSIONS

Analysis of Public Awareness

A total of 336 respondents were involved in the survey to evaluate FOG management practices and levels of awareness in the pre-determined premises. Table 4 shows the demographic analysis of the respondents

Table 4
Demographic of respondents

Demographic	Population (n)	Percentage (%)
Types of premises		
Hotels	175	52.1
Shopping malls	161	47.9
Categories of respondents		
Food operators	207	61.6
Administration	129	38.4
Level of education		
Malaysian Certificate of Education (*Sijil Pelajaran Malaysia (SPM)*)	81	24.1
Diploma	132	39.3
Degree	117	34.8
Masters	6	1.8

175 respondents (52.1%) work in the hotel industry, while 161 (47.9%) were shopping mall employees. Further breakdown amongst the respondents shows that 38.4% (129 respondents) are from the management, whereas 61.6% (207 respondents) are food operators. Management refers to supervisors and those working in an office environment, whereas operators are those working in the kitchen or dealing directly with customers. A huge difference in the breakdown can be noticed as there are generally a small number of people in the management team per venue. In contrast, food operators at any single premises would be on the higher side due to the number of kitchens per venue.

It was found that most respondents are diploma (39.3%) and degree (34.8%) holders, and only 6 are Master's degree holders. Upon further investigation among the diploma holders, 35.6% were at a management level, and 64.4% were food operators. Through verbal communication, it was deduced that a high number of food operators were diploma holders working part-time jobs while awaiting further education. In management, it can be commended that those with a diploma were able to work rank and file to reach a management level. Among the degree holders, 68.4% were at a management level, and 31.6% were food operators. The degree holders could be working as part-time food operators to earn extra income or while waiting for a permanent job offer. 100% of Master's degree holders were from the management level. Figure 2 shows the level of education among the management

team and food operators. It can be concluded that most management teams hold a degree or at least a diploma, while the food operators are school leavers with a secondary school certificate or diploma holder.

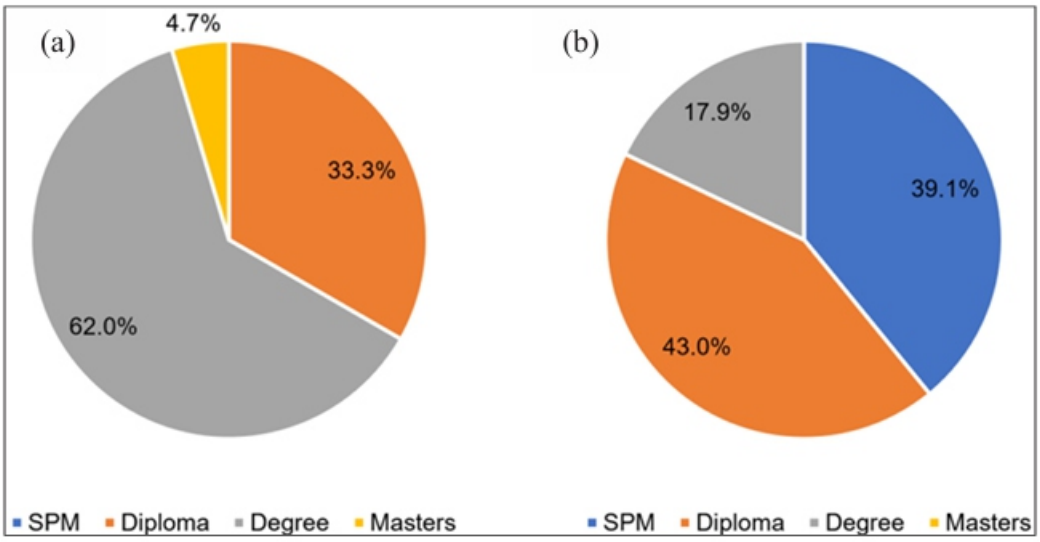

Figure 2. Level of education among the respondents: a) management, b) food operators

Successful control and management of FOG is largely dependent on public awareness and a clear understanding of its impact on the environment. Table 5 shows respondent's awareness of FOG in general. The survey revealed that 85% of the respondents understood that FOG is a by-product of food preparation and production and that food service establishments are a significant source of FOG. Although 14% of the respondents are uncertain about the substance, all respondents are well aware that their premises are producing FOG.

Waste cooking oil (WCO) consists of oils and fats used for cooking or frying in the food processing industry, food handling businesses, and households. Although both WCO and FOG are by-products from food establishments, collecting WCO is much easier and can be recycled to make soap, lubricants, candles, animal and pet feed as well as renewable energy (Awogbemi et al., 2021). Considering that WCO has become a valuable commodity and may constitute a great proportion of FOG, respondents were enquired on the difference between WCO and FOG. 81.6% were aware of the difference and understood that pouring WCO down the kitchen sink and into the drain is detrimental to the environment. The Star has reported that in 2016, Klang Municipal Council spent almost RM6 million to remove clogging caused by hardened cooking oil in drains (Edward, 2016).

Drainage systems in food processing facilities can experience a build-up of FOG. When FOG is allowed to go down the drain, it solidifies, reducing and preventing water f low in drains and sewer pipes, causing sewage backups and overflows, leading to property damage, environmental problems, and other health hazards (Owolabi et al., 2022). This survey revealed that 83.1% of the respondents agree that FOG

is a potential environmental threat if disposed of inappropriately. However, only 67.6% knew that the Housing and Local Government Ministry made it a requirement since 2005 for all food premises to install, maintain and desludge grease trap systems to obtain or renew business licenses. Under the present guidelines, restaurant operators must clean and dislodge a grease inceptor installed at their premises once every two weeks. The remaining respondents were unaware of any rules or regulations imposed by the government.

Table 5
Respondent's awareness of FOG

Awareness	Population, n (total 336)				
	Strongly agree	Agree	Neither agree nor disagree	Disagree	Strongly disagree
FOGs are by-products from food preparation and production	276 (82.1%)	10 (3.0%)	3 (0.9%)	47 (14.0%)	0
FOG is produced in the premise	322 (95.8%)	14 (4.2%)	0	0	0
FOG differs from WCO (waste cooking oil)	260 (77.4%)	14 (4.2%)	2 (0.6%)	60 (17.9%)	0
FOG has a negative impact on the environment	261 (77.7%)	18 (5.4%)	20 (6.0%)	37 (11.0%)	0
Rules and regulations exist related to FOG	219 (65.2%)	8 (2.4%)	25 (7.4%)	84 (25.0%)	0

The median was calculated for the data set, and it was found that 81.2% of the total respondents perceived awareness of FOG, and 18.5% can be considered neutral. Only 0.3% of respondents had very limited knowledge of FOG. Crosstabulation between the median and categories of respondents found that 98.44% of the management personnel have an awareness of FOG, compared to 70.53% among the food operators.

FOG management is vital to running an efficient, hygienic and compliant kitchen. Typically, a grease trap is used as a receptacle into which wastewater containing FOG f lows before entering a drainage system. From Table 6, all respondents reported that their premises installed individual grease traps and that FOG produced at their premises was channeled to these grease traps and subsequently to a communal grease trap. However, a small number of businesses chose to pour FOG into containers and dispose of it in the bin once it had hardened, as reported by six respondents. Also, 6% of the respondents admitted that their premises flushed the FOG down the drains and sinks and into the sewer system. This may cause sanitary sewer overflows, which are clogs in the collection systems, that can potentially result in raw sewage being released into communities, causing potentially dangerous health conditions

(Owolabi et al., 2022). Although the numbers are not alarming, food establishments should make conscious efforts to dispose of FOG safely. There are a plethora of ways restaurants and eateries can stop FOG from going down the drain and into the sewer. Even making small changes, such as wiping down plates and pans with paper towels, can make a huge difference in washing areas of kitchens, where blockages frequently occur in the sink units.

The types of cleaning agents most commonly used in commercial kitchens are detergents, degreasers, abrasives and acids. Detergents are usually neutral chemicals with pH 6-8 and contain surfactants to break up dirt or soil for easy washing. Degreasers remove grease from surfaces such as oven tops and counters, while abrasives are usually used to clean floors, pots and pans. Acids are the most powerful type of cleaning agent and are usually used to clean drains and sinks in the kitchen as well as descaling the dishwashers. From this survey, 96.7% of total respondents agreed to use the stated chemicals in their premises. The use of acids and alkaline can potentially cause damage to the pipes as well as alter the constituents of the FOG. Detergents in background water increase the production of calcium-based saponified solids that may clog sewer lines and eventually cause sanitary sewer overflows (Iasmin et al., 2016). The use of detergents and sanitizers may also affect the emulsification characteristics, such as the droplet size of FOG discharges, and thus impact the separation ability in the grease trap (Sello, 2021).

Table 6
Respondent's awareness of FOG management in the premise

Awareness	Population, n (total 336)				
	Strongly agree	Agree	Neither agree nor disagree	Disagree	Strongly disagree
The presence of a grease trap in the premise	316 (94.0%)	20 (6.0%)	0	0	0
FOG is channeled directly to the grease trap	316 (94.0%)	20 (6.0%)	0	0	0
FOG is discarded into the dustbin	0	6 (1.8%)	19 (5.7%)	311 (92.6%)	0
FOG is flushed into the sewer line	0	20 (6.0%)	18 (5.4%)	298 (88.7%)	0
Chemicals are used as cleaning materials in the kitchen	293 (87.2%)	32 (9.5%)	11 (3.3%)	0	0

Based on the median, 76.2% of the respondents perceived awareness of FOG management in their premises. Crosstabulation between the median and categories of respondents found that 85.3% of management respondents understood good FOG management practices, whereas only 70.5% of food operators practiced good FOG management.

Restaurants and the food processing industry are the main sources of FOG; therefore, it important that the grease traps used at these establishments are effective in removing the substance from wastewater before entering the sewer system. Ensuring that grease traps are properly installed and, most importantly, properly maintained is challenging. Poorly maintained and low capacity of grease traps will allow FOG to flow into the sewer pipes, causing the build-up of fatberg. A fatberg is a coagulated mass of congealed grease and non-biodegradable matter found in sewers and drains that cause extensive damage to drainage systems (Abdullah, 2021).

The principal constituents of concern for restaurant wastewater are its organic strength (BOD and COD), particulate loading (TSS), and oil and grease (O&G). The strength of the wastewater is affected by many factors, including cuisine type, kitchen capacity, grease trap size and FOG management practices (Gurd et al., 2019). Ultimately, the effluent from food establishments must meet certain discharge limits before entering the public sewer system. Figures 3 and 4 show the BOD and COD values for communal grease traps at selected hotels and shopping malls for both influent and effluent streams. As evident from Figure 3, all premises have exceeded the allowable BOD discharge limit of 250 mg/L. Unexpectedly, BOD values of the effluent for most premises were found to increase from the influent values, which indicated that the effluent was contaminated with high organic loading. Only one hotel premise, H1, was able to remove 40% of BOD compared to four shopping malls (S4, S5, S6 and S7) that were able to remove as low as 3% to 75% of BOD. Figure 4 shows similar observations for COD where concentrations at the effluent were higher than the influent and exceeded the permissible limit of 500 mg/L. The highest level of COD for hotel effluent was almost 30000 mg/L, while for shopping malls, soar to 93000 mg/L. Although some communal grease traps at the shopping malls (S4, S5, S6 and S7) were able to treat between 5% to 62% of COD, the final effluent still did not meet the discharge requirement. This indicates that the grease traps did not work as anticipated.

It has been reported that grease traps are capable of removing up to 80% of FOG from the influent. However, little evidence was presented for BOD and COD removal. A study by the United States Environmental Protection Agency (U.S. EPA) reported that the grease trap unit was able to remove 26%–65% of BOD, 40%–80% of TSS and 70%–80% of FOG, while a laboratory scale study proved that grease traps can remove 50%–80% of BOD and TSS (U.S. EPA, 2012; Wongthanate et al., 2014). The incapability of grease traps to treat BOD and COD usually stems from a lack of timely servicing and poor maintenance. A regular grease trap cleaning schedule prevents FOG from building up and ensures that the trap continues to operate effectively. Also, the inadequate size of the grease trap may cause insufficient retention time for organic/inorganic matter breakdown, leading to significant variations of BOD and COD.

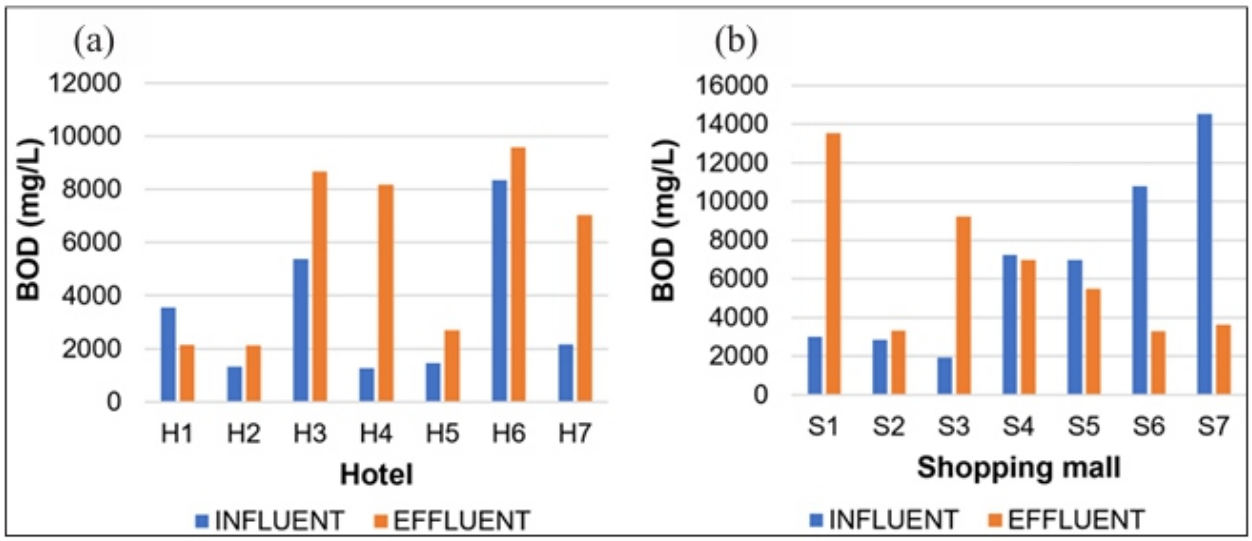

Figure 3. BOD results for communal grease traps at (a) hotels and (b) shopping malls

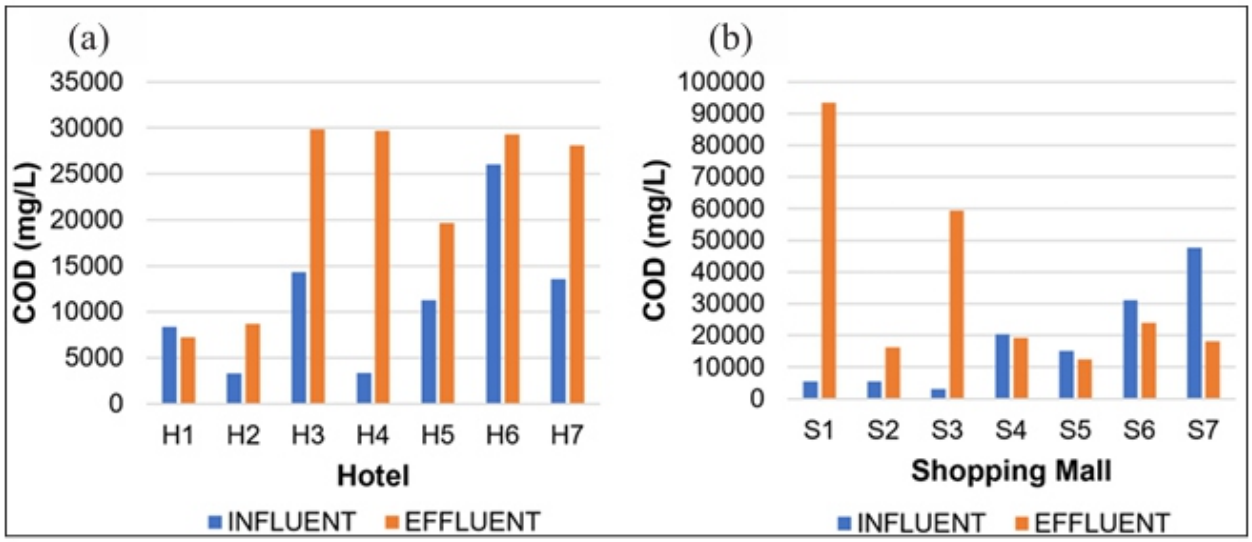

Figure 4. COD results for communal grease traps at (a) hotels and (b) shopping malls

High COD in water indicates greater levels of oxidizable organic matter and, consequently, a lower amount of DO. All hotels and shopping malls depict a DO reading of less than 1 mg/L before and after the grease trap, which indicates a symptom of excessive contamination. Low dissolved oxygen may result from high water temperature and suspended solids. It is well known that food premises use hot water together with acidic cleaning agents to clean utensils and the kitchen at the end of the operation. When there is a rise in effluent temperature due to the discarded hot water during the cleaning process, the suspended solids will absorb the heat and decrease the DO levels (Mutalib et al., 2015). Also, hot water holds less DO compared to cold water (Bozorg-Haddad et al., 2021). The presence of O&G in the grease trap forms an impenetrable layer above the effluent surface. This decreases interaction in the open air and thus reduces the DO level in the effluent. Grease traps are usually situated in secluded areas of the

hotel and shopping mall premises due to bad odor and unexpected backflow or flooding. It is usually not in an open area with adequate air circulation, thus reducing the opportunity for any sort of sunlight, natural aeration or ventilation.

As presented in Figure 5, all premises have exceeded the allowable discharge limit of 50 mg/L for O&G. Three of the hotel premises (H1, H3 and H4) were able to reduce the O&G content between 39% to 65%, and three of the shopping malls (S3, S4 and S6) were able to remove 25%–83% of the O&G. The rest of the grease traps in both hotels and shopping malls showed an increment of O&G content in the effluent. Ideally, the O&G content should be reduced when subjected to an efficient working condition of the grease trap, as it would stay afloat in the first and second chambers. FOG is derived from many organic non-polar compound food sources with a density of approximately 0.863–0.926 g/cm3 (Wallace et al., 2017; Ali et al., 2022), while water is a polar solvent which has a density of 1.000 g/cm3. Hence, density and polarity contribute towards the floating of FOG over water. Issues occur when high water temperatures are used for washing and cleaning in the kitchen. The heating of oils causes FOG to liquefy, emulsify and react with other organic compounds, thus changing the chemical composition of FOG and its polarity.

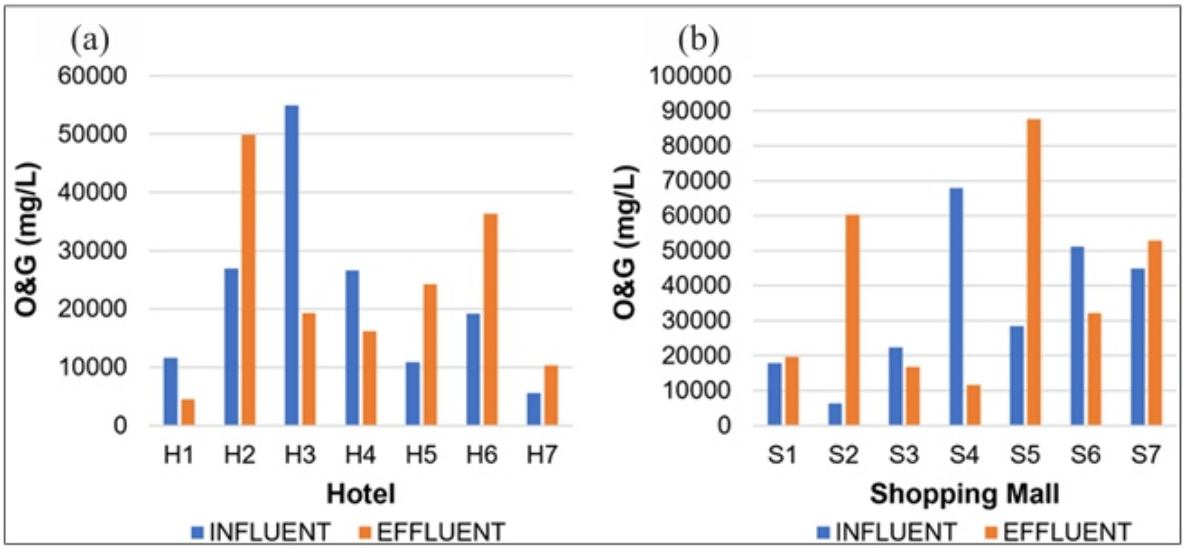

Figure 5. O&G results for communal grease traps at (a) hotels and (b) shopping malls

Compared to hotel premises, the shopping malls are bigger in size; for this reason, the content and quantity of the O&G differs greatly between the two premises. The quality of the effluent also differs depending on the type of grease traps used in the premises and the frequency of service. The type of grease trap plays a vital role in ensuring that the O&G is retained in the first and second chambers while the water exits the grease trap through the outlet pipe. In this study, hotel H2 has been in the industry for 40 years and operates with concrete-based grease traps with only two chambers. The baffles are worn out, and the concept of O&G retaining them in the first chamber is almost impossible. The in the grease trap is the integral component that serves to slow down the flow of and lengthen the detention time to

maximize the separation of the FOG and settling of the solids (Hendrasarie & Maria, 2021). The failure of the grease trap is clearly depicted in the O&G effluent value, which increased significantly by almost 84.7%. Similarly, hotel H5 has an increased O&G effluent value of almost 122.3% as it uses a grease trap of insufficient size.

Be it a hotel or a shopping mall, items discarded into the kitchen sink vary from cooking oil to organic materials such as food waste, raw materials, meats, margarine and flour. The pipelines carry this waste through its channel to the respective grease traps. High grease loads, emulsified grease, and fast flow volume have caused FOG to bypass the grease trap and discharge in the effluents. Grease traps with a higher frequency of service will have O&G concentrated in the first and second chambers, whilst the third chamber would only contain clouded water with minimal oil traces floating. In comparison with grease traps that are serviced monthly or bi-monthly, traces of O&G will be evident in all three chambers and can be seen flowing out via the outlet as well when agitated. With timely service, the O&G will be removed, and the process will stay efficient.

High TSS values in the effluent are often related to excessive solids generation due to an increase in BOD loading. Figure 6 shows that the TSS values in the effluent for both hotels and shopping malls range from 10,000 mg/L to 72,000 mg/L. Grease traps at the shopping malls S4, S5, S6 and S7 could reduce 39%–88% of the TSS, while a very low removal rate was observed for hotel grease traps (H3 and H7). The high flow rate of the influence was found to affect the TSS removal, although the same could not be said for BOD and FOG removal.

Solids in the grease trap may originate from different areas of the premise. In some premises, the kitchen pipelines are shared amongst floor traps, stove areas, food preparation areas, sink pipelines, and dishwashers, which end up in the grease trap. Apart from the organic compound, other materials are discarded into the pipeline that contributes to the significant level of TSS in hotels and shopping malls, such as cleaning the kitchen flooring, which results in dirt, sand, and even sometimes gravel-washed into the pipeline. Another important factor to consider is that the grease trap main pipeline is usually made of cast iron or PVC pipes. Over time, cast iron pipes tend to corrode due to the use of acidic cleaning agents and the rodding process that scrapes the inner layer of the pipe and releases metal particles. As the effluent passes through these pipes, the above residues join the affluent and end in the grease traps, which was the case with hotels H3, H6 and H7 and shopping malls S4, S6 and S7.

At the grease trap itself, there were signs of damage due to wear and tear and evidence of corrosion, which further contributed to the increment of TSS values in the effluent stream. Furthermore, if the grease traps are made of old traditional concrete design, they are more likely to have sand, silt, and gravel residue in the grease trap, as in the case of hotel H2. Also, the grease traps are usually located in the basement or car park areas, with significant amounts of sand, silt, dried leaves and dirt escaping into the grease traps due to vehicle movement. Although the grease traps are covered, the contractors will lift the lid during scheduled servicing, which causes these elements to fall into the traps.

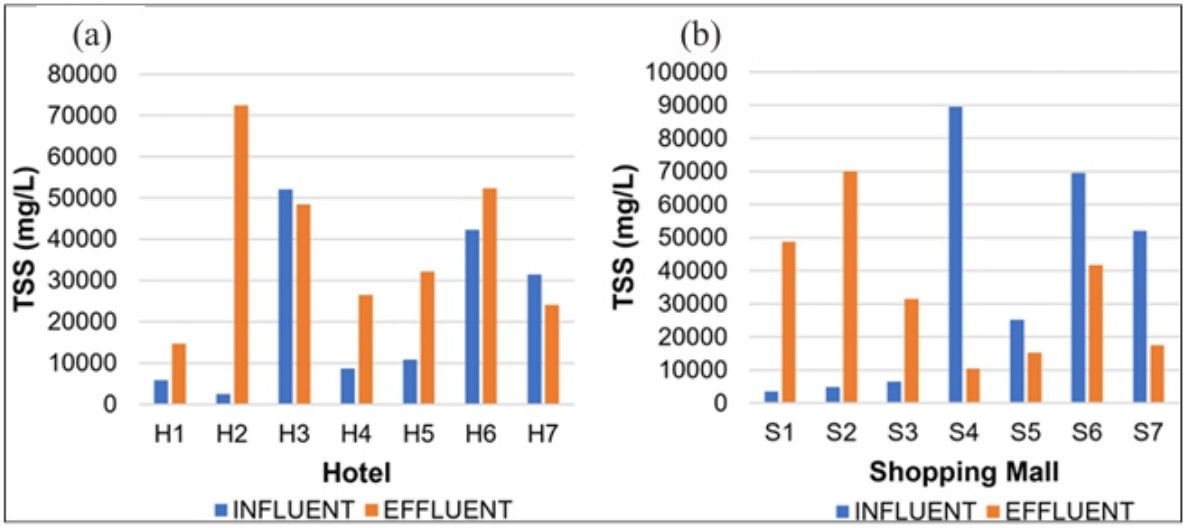

Figure 6. TSS results for communal grease traps at (a) hotels and (b) shopping malls

The permitted pH value of effluent in the sewer network is between pH 6.0 to 9.0. As shown in Figure 7, all hotels and shopping malls recorded a pH value of less than 6.0, which is acidic and not permissible to be discharged into the sewer network. FOG in the grease trap will begin to float as the influent cools down, after which it will start to break down

by hydrolysis, where the fatty acids are released. The decrease in pH value is a result of the release of a significant volume of free fatty acids (FFA), which eventually will cause corrosion inside the grease trap (Husain et al., 2014). Also, food operators in hotels and shopping malls are usually instructed to wash and discard all wastewater via the sink, which connects to the floor trap pipeline. By the same token, during closing hours, the workstations, food preparation tables, floors and sinks are washed down using cleaning agents, which are commonly acidic.

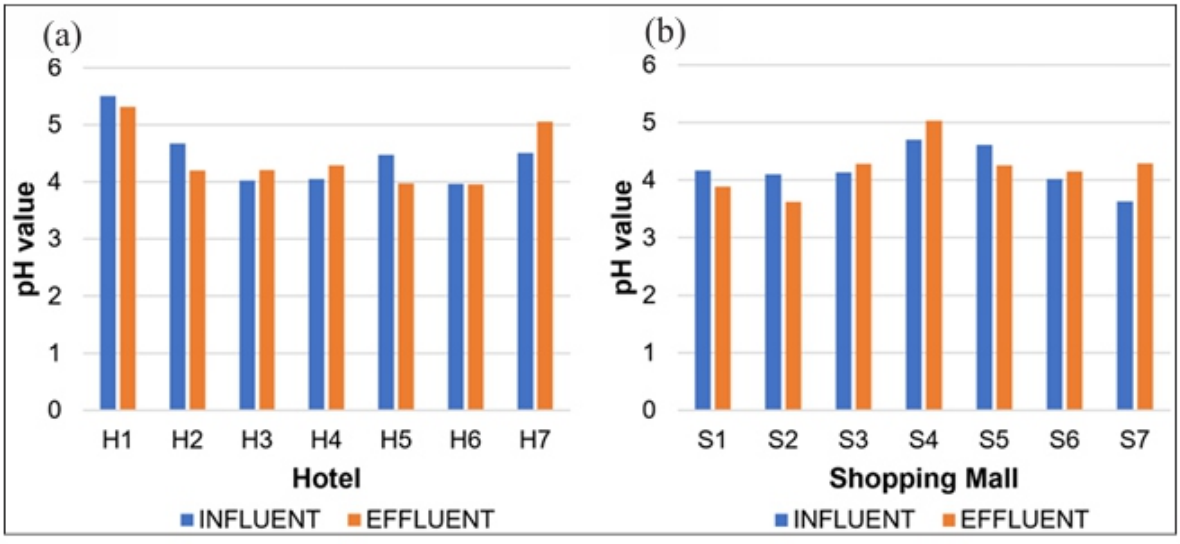

Figure 7. pH values for communal grease traps at (a) hotel and (b) shopping malls

An improper discard of organic food wastes into the pipeline will end up in the first chamber basket. Depending on the frequency of service, this food waste will remain in the grease trap basket and begin to decompose. Organic matter, such as vegetables and meat products, contains carbon elements, which will be released into the effluent decomposition. Due to the instability of these organic compounds and their ability to be easily oxidized, carbon dioxide will be produced. As a result, the dissolved carbon will increase the hydrogen ions, causing the pH value to decrease, denoting its acidity.

In addition, certain kitchens and floor traps may experience the gargling effect or slow exit as foreign materials may build up or harden FOG, which reduces the pipe's clearance for a smooth effluent flow out. At this point, it is a common practice in hotels and shopping malls to pour acid-based FOG cutters into these floor traps to help them clear the line. This is a quick fix in practice that helps hotel, and shopping mall kitchen operators expedite the cleaning process. Another factor that causes an increase in effluent acidity is the dumping of cleaning agents into the grease trap by unauthorized personnel. The housekeeping personnel are usually scheduled to clean the grease trap area as it is commonly used as temporary storage. The housekeepers dumped the leftover solutions into the grease traps for convenience during the cleaning process using acidic detergents and cleaning agents.

CONCLUSION

Awareness among those working within food service establishments determines the success or failure of the FOG management initiatives. In this work, we reported that 81.2% of the respondents had a perceived understanding of FOG, while 76.2% possessed an of how it is managed within their premises. The awareness level is independent of job position; however, a vast majority of the respondents who work in management are more acquainted with the knowledge of FOG and its management compared to the operators. Further investigation of the communal grease traps at selected hotels and shopping malls revealed that none of the effluent parameters met the permissible discharge level stipulated in the Water Services Industry (Prohibited Effluent) Regulations 2021 (Regulation 4). The highest level of O&G for hotel and shopping mall effluents were 50000 mg/L and 85000 mg/L, respectively, while TSS values in the effluent range from 10,000 mg/L to 72,000 mg/L. This important finding demonstrates poor design, maintenance, and monitoring of the grease traps by the premises owner and local authorities. Further work will be focusing on upgrading the conventional grease trap to a smart grease trap with sensor incorporation that will enable accurate level measurements and an effective alarm system to indicate the user and contractor for maintenance services.

ACKNOWLEDGEMENT

This work was financially supported by Geran Universiti Putra Malaysia (Project code: GP-

-IPS/2023/9743500).

REFERENCES

Abdullah, N. I. (2018). Grease Trap Helps to Prevent Environmental Problems. Federation of Malaysian Consumers Associations. https://www.fomca.org.my/v1/index.php/fomca-di-pentas-media/fomca-di pentas-media-2018/268-grease-trap-helps-to-prevent-environmental-problems

Ahmad, I., Abdullah, N., Koji, I., Yuzir, A., Ahmad, M. D., Rachmadona, N., Al-Dailami, A., Show, P. L., & Khoo, K. S. (2023). Micro and macro analysis of restaurant wastewater containing fat, oil, grease (FOG): An approach based on prevention, control, and sustainable management. Chemosphere, 325, Article 138236. https://doi.org/10.1016/j.chemosphere.2023.138236

Ali, M. A. H., Talib, S. H. A., & Hashim, S. I. N. S. (2022). The combination of a previous kitchen waste grease trap for fat, oil, and grease for pre-treatment. Journal of Advancement in Environmental Solution and Resource Recovery 2(2), 37–43.

Awogbemi, O., Von Kallon, D. V., Aigbodion, V. S., & Panda, S. (2021). Advances in biotechnological applications of waste cooking oil. Case Studies in Chemical and Environmental Engineering, 4, Article 100158. https://doi.org/10.1016/j.cscee.2021.100158

Aziz, T. N. (2010). Analysis of Grease Abatement Devices and the Measurement of Fat, Oil, and Grease in Food Service Establishment Waste Streams. (PhD dissertation). North Carolina State University, USA. http://www.lib.ncsu.edu/resolver/1840.16/4395

Aziz, T. N., Holt, L. M., Keener, K. M., Groninger, J. W., & Ducoste, J. J. (2011). Performance of grease abatement devices for removal of fat, oil, and grease. Journal of Environmental Engineering 137(1), 84–92. https://doi.org/10.1061/(ASCE)EE.1943-7870.0000295

Bozorg-Haddad, O., Delpasand, M., & Loáiciga, H. A. (2021). Water quality, hygiene, and health. In O. Bozorg Haddad (Ed.), Economical, Political, and Social Issues in Water Resources (pp. 217-257). Elsevier. https:// doi.org/10.1016/B978-0-323-90567-1.00008-5

Chinwetkitvanich, S., & Ektaku, P. (2020). Reality in package on-site grease trap performance: Success and failure in fog removal. GEOMATE Journal, 18(67), 156-161.

Collin, T., Cunningham, R., MacAdam, J., Villa, R., Jefferson, B., & Jeffrey, P. (2023). Towards a risk ranking for improved management of discharges of fats, oils, and greases (FOG) from food outlets. H2Open Journal, 6(1), 29-39. https://doi.org/10.2166/h2oj.2023.056

Edward, R. (2016, December 7). MPK Spent Close to RM6mil to Remove Hardened Cooking Oil from Drains. The Star. https://www.thestar.com.my/metro/community/2016/12/07/expensive-mess-to-clean-mpk-spentclose-to-rm6mil-to-remove-hardened-cooking-oil-from-drains/

Gurd, C., Jefferson, B., & Villa, R. (2019). Characterisation of food service establishment wastewater and its implication for treatment. Journal of Environmental Management, 252, Article 109657. https://doi. org/10.1016/j.jenvman.2019.109657

He, X., de los Reyes, F. L., & Ducoste, J. J. (2017). A critical review of fat, oil, and grease (FOG) in sewer collection systems: Challenges and control. Critical Reviews in Environmental Science and Technology 47(13), 1191–1217. https://doi.org/10.1080/10643389.2017.1382282

Hendrasarie, N., & Maria, S. H. (2021). Combining grease trap and Moringa oleifera as adsorbent to treat wastewater restaurant. South African Journal of Chemical Engineering, 37, 196-205. https://doi.org/10.1016/j.sajce.2021.05.004

Husain, I. A. F., Alkhatib, M. F., Jammi, M. S., Mirghani, M. E. S., Zainudin, Z. B., & Hoda, A. (2014).Problems, control, and treatment of fat, oil, and grease (FOG): A review. Journal of Oleo Science 63(8), 747–752. https://doi.org/10.5650/jos.ess13182

Iasmin, M., Dean, L. O., & Ducoste, J. J. (2016). Quantifying fat, oil, and grease deposit formation kinetics. Water Research, 88, 786-795. https://doi.org/10.1016/j.watres.2015.11.009

KPKT. (2017). Garis Panduan Pemasangan Perangkap Minyak di Premis Makanan di Kawasan Pihak Berkuasa Tempatan [Guidelines for the Installation of Grease Traps in Food Premises under the Local Authorities Area]. Kementerian Perumahan dan Kerajaan Tempatan. https://mpkulai.gov.my/wp-X/uploads/2024/05/garis_panduan_pemasangan_perangkap_minyak_di_premis_makanan_di_kawasan_pihak_pbt_kpkt.pdf

Mutalib, N. A. A., Karim, O. A., & Mustafa, A. D. (2015). The water quality study and sources of pollution in Alur Ilmu, UKM. Malaysian Journal of Analytical Sciences, 19(5), 1137-1146.

Nieuwenhuis, E., Post, J., Duinmeijer, A., Langeveld, J., & Clemens, F. (2018). Statistical modelling of fat, oil and grease (FOG) deposits in wastewater pump sumps. Water research, 135, 155-167. https://doi.

org/10.1016/j.watres.2018.02.026

Owolabi, T. A., Mohandes, S. R., & Zayed, T. (2022). Investigating the impact of sewer overflow on the environment: A comprehensive literature review paper. Journal of Environmental Management, 301,Article 113810. https://doi.org/10.1016/j.jenvman.2021.113810

PUB. (2017). Code of Practice on Sewerage and Sanitary Works. Public Uitilities Board. https://www.pub.gov.sg/-/media/PUB/PDF/Compliance/Used-Water/GreaseTrap/COPSSW2nded2019.pdf

Sello, M. (2021). Wastewater fats oils and grease characterisation, removal and uses. A review. Environmental Science: An Indian Journal 17(10), Article 200.

Straub, D., Boudreau, M. C., & Gefen, D. (2004). Validation guidelines for IS positivist research. Communications of the Association for Information Systems, 13, 380-427. https://doi.org/10.17705/1CAIS.01324

Sultana, N., Roddick, F., Gao, L., Guo, M., & Pramanik, B. K. (2022). Understanding the properties of fat, oil, and grease and their removal using grease interceptors. Water Research, 225, Article 119141. https:// doi.org/10.1016/j.watres.2022.119141

Tang, L. Y., Wong, N. H., Am Chieng, T., Kiu, A. K. J., Choo, C. S., Li, Y., Tan, C. P., Yaser, A. Z., Khaerudini, D. S., Chen, G. H., & Sunarso, J. (2024). Physicochemical characteristics of grease-trap wastewater with different potential mechanisms of FOG solid formation, separation, and accumulation inside grease traps. Water Research, 256, Article 121607. https://doi.org/10.1016/j.watres.2024.121607

U.S.EPA. (2012). Design Manual: Onsite Wastewater Treatment and Disposal System. United States Environmental Protection Agency. https://www.epa.gov/sites/default/files/2015-06/documents/2004_07_07_septics_septic_2002_osdm_all.pdf

Wallace, T., Gibbons, D., O'Dwyer, M., & Curran, T. P. (2017). International evolution of fat, oil and grease (FOG) waste management - A review. Journal of Environmental Management 187, 424–435. https://doi. org/10.1016/j.jenvman.2016.11.003

Water UK. (2017). Disposal of Fats, Oils, Grease and Food Waste - Best Management Practice for Catering Outlets. Water UK. https://www.aquariusgroup.co.uk/wp-content/uploads/2018/03/Disposal-of-Fats Oils-Grease-and-Food-Fats.pdf

Wongthanate, J., Mapracha, N., Prapagdee, B., & Arunlertaree, C. (2014). Efficiency of modified grease trap for domestic wastewater treatment. The Journal of Industrial Technology, 10(2), 10-22.

ISSN 0128-7680

Random Forest Model for Software Build Time Prediction on CI/ CD Pipeline

Wen Han Seow1, Chia Yean Lim1* and Sau Loong Ang2
1School of Computer Sciences, Universiti Sains Malaysia, 11800, Minden, Pulau Pinang, Malaysia
2Department of Computing and Information Technology, Tunku Abdul Rahman University of Management and Technology, Penang Branch, 11200, Tanjung Bungah, Pulau Pinang, Malaysia

ABSTRACT

In the fast-paced world of software engineering, Continuous Integration/Continuous Delivery (CI/ CD) pipelines are essential to deliver software builds continuously. However, the varying time taken for software builds to complete on these pipelines can challenge scheduling software delivery and impact productivity. To the best of researchers' knowledge, machine learning techniques have never been used to predict software build time in the CI/CD pipeline. This research attempted to apply data science and machine learning techniques, including linear regression (LR), support vector regressor (SVR), random forest regressor (RFR), and XGBoost regressor, to predict software build completion time to address this research gap. Past build events were used as a dataset to train and identify the best-performing model by evaluating the time a software build takes to complete. Different factors contributing to software build time on the CI/CD pipeline were also analyzed to identify opportunities for improvement. This research found that the random forest (RF) model achieved the best and outstanding performance of 14.306 in mean squared error (MSE). This model could be deployed to provide completion time estimates for software builds, enabling better code delivery scheduling. This research also suggested opportunities for improvement in the CI/CD pipeline by discovering major factors causing high build time in the CI/CD pipeline that engineers could rectify to reduce software build time in the CI/CD pipeline.

Keywords: *CI/CD, machine learning, random forest, regression, software engineering*

I. INTRODUCTION

Continuous Integration/Continuous Delivery (CI/CD) is a method of frequently delivering applications or software by introducing automation into the stages of software development (Red Hat, 2023). In short, new software codes submitted by the software engineers will go through a pipeline consisting of several stages of processes defined with steps to be tested and built, then proceed to deployment into the production environment. This method was widely used in software development companies of all sizes.

At this point in time, CI/CD is no longer a stranger to the software engineering field and has been widely adapted into the software development process across companies and industries. Benefits such as

ensuring code quality, delivering codes faster with accelerated release rate, simplified rollback and cost reduction are among the top reasons companies adopt CI/CD (Silverthorne, 2022). In a study aimed at investigating how CI/CD adoption can impact open-source repositories hosted on GitLab and GitHub, it was found that adoption of CI/CD enhanced commit velocity by 141.19% in more than 12,000 repositories (Fairbanks et al., 2023).

A survey conducted by JetBrains showed the importance of CI/CD. 44% of the participants confirmed regular usage of CI/CD tools, and a significant 22% of them even adopted a new CI/CD tool within the past year (Bedrina, 2023). Since the usage of the CI word back in 1991, CI/CD has evolved from a relatively niche practice into an industry standard (Snyk, 2020).

In software development companies, the developer productivity (DevProd) team often aims to enhance the overall software development process and environment for all software engineers. Factors such as software tools and their configurations, development environments, cloud services like Amazon Web Services (AWS) and most importantly, the CI/CD framework could affect the software's build time in their own way (Amazon Web Services, 2023). With the size of an established technology company, more and more software engineers would join the company, and the number of software products would grow daily. There is no doubt a pressing need to improve the productivity of software engineers by streamlining their daily jobs.

There have always been issues in the availability and reliability of CI/CD and the unsatisfactory performance of software build time on the CI/CD pipeline has led to concern among the DevProd team and software engineers in the software development company. Software engineers in the company approach the DevProd team regularly for support and troubleshooting problems during their daily software engineering work. DevProd team has also continuously made an effort to improve the quality of service of the CI/CD pipeline to benefit the company's software production efficiency. Hence, the continuous effort to find ways to further optimize the CI/CD quality of service is never ending.

It was discovered that data science techniques can be used to eradicate the existing software build time issues in the CI/CD pipeline. In a multi-national software development company, the DevProd team has collected the data and logs of software build events for a long period. Information such as time start, time end, region, and operating system were collected and archived on data platforms for data-keeping purposes. With the dataset

being stored and kept unused, the company now sees a chance to use it well. Data science techniques can be applied to the dataset for further analysis, achieving the goal of providing a better software development experience for the company. To the best knowledge of literature searching, no prior research was conducted on applying methods on CI/CD pipelines to predict software build time and analyze the major factors causing high software build time.

This research was conducted by applying several data science techniques to find out the causes behind the CI/CD pipeline's flaky service quality while utilizing the dataset to train a machine learning model that predicts the estimated time taken by a software build. Data analysis efforts were carried out to look for factors behind the unusually long software build time and availability issues of the CI/CD service. Supervised machine learning methods like regression can be applied to predict the estimated time the software build takes to complete. It not only saves software engineers time by giving them an expectation of time for their software build to complete in the CI/CD pipeline but also enables software engineers to plan their tasks better by hand. When it comes to urgent bug fixes and patches where deployments are expected to happen as soon as possible, the estimated build time will be helpful for the software team to anticipate the successful build to go live on production.

With the predicted output of the machine learning model on the estimated time taken of software build, anomaly build events that end prematurely or take extended time will be detected and then reported to the DevProd team. The team could immediately look after the CI/CD pipeline and respond when anomalies happen. A variety of reasons could lead to CI/CD pipeline issues and out-of-ordinary software build times. However, these issues could be investigated and rectified swiftly if identified instantly. The research hopes not only to benefit the DevProd team and the software company but also to discover and study the possibility of applying data science and machine learning techniques to the areas of software build data on the CI/CD pipeline. It is crucial to software development productivity because it would greatly reduce engineering effort, money, and time.

Literature Review

Continuous Integration (CI) and Continuous Delivery (CD)

Continuous Integration (CI) is a software development practice where the software engineers merge new codes into the remote code repository (such as GitHub) regularly; the automated builds and tests are running in a usually cloud-hosted CI pipeline instead of the software engineer’s local development environment (Amazon, 2023). CI saves the software engineer’s effort and time by running the software builds and tests over the centralized pipeline, where the CI pipeline is usually the single source of truth on whether the build has passed the tests and is good to go for deployment into production.

Continuous Delivery (CD) is the process where new software codes are automatically built, tested and released into production continuously (Amazon, 2023). It is important to ensure the code changes are fit for going into the production environment with the help of a series of automated software tests. The

stages of the CI/CD process are shown in Figure 1.

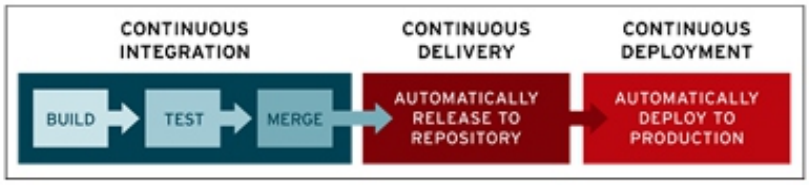

Figure 1. Stages of CI/CD Process (Red Hat, 2023)

When the DevProd team has already integrated the CI/CD pipeline by involving a wide range of AWS services and other Software as a Service (SaaS) products such as Buildkite, project development will be easier after understanding how the products interact with the CI/CD pipeline that has been serving the company's software engineers.

Contrary to what most believe, the build time of software impacts a software developer's productivity more than most people would imagine. By accurately providing the estimated build time, developers could have better control over their time planning and organizing their tasks based on the predicted build time of software on the CI/CD pipeline. For example, the developer may go for a lunch break when the build is predicted to take around an hour. When the build is expected to take 5 minutes, the developer may proceed to check the emails or go for a quick code review. The essence is to come up with a build time prediction that is accurate enough for developers to gain control of time and optimize the tasks in their hands (Jaspan & Green, 2023). Ultimately, it brings more efficiency into daily tasks by reducing time wasted waiting for the software build to be completed or time spent on miscellaneous tasks when the software build has already been completed.

Google conducted an in-house experiment to measure how the improvement of software build time affects developer satisfaction (Jaspan & Green, 2023). In the experiment group, developers were equipped with performant machines that outperformed the control group machines by a modest 15%. The results of the experiment have shown that developers managed to achieve higher self-reported productivity and higher self-reported velocity in their work. Developers in the experiment group also measured a greater satisfaction level than the control group. It is a concrete example of how faster build time could bring benefits to developers and the company.

CI/CD pipelines are not easy to troubleshoot. The time taken for software to build on a CI/CD pipeline could fluctuate due to many factors, including machine specification, agent availability, and CI/CD pipeline configurations. Engineers spend much time daily discovering the reasons that have caused inconsistency or even a spike in software build time on the CI/CD pipeline. The action taken to remedy the issue may not always be the best action to resolve the issue. It is challenging to quickly come up with the right solution to fix the slow-performing CI/CD pipeline. While there are no existing machine learning methods to help in the prediction of the CI/CD pipeline build time and discovering the factors

affecting the build time, the effort to optimize the build time is always based on conventional and traditional methods such as expert knowledge, software engineer's best guessing, or finding similar solution from online sources. The current methods are illustrated in Table 1

Table 1
Comparison between current methods of debugging CI/CD pipeline

Current Method	Methodology	Weakness
Expert knowledge	Experts will diagnose the issue based on experience and domain knowledge	Highly dependent on having an experienced expert with deep domain knowledge
Engineer's guessing	Engineers debug based on their guessing and experience	Guessing may be inconsistent and unreliable
Finding solutions from online Sources	Engineers look for possible solutions from online sources, such as forums, to fix the issue	It is time-consuming to look for solutions from different sources Unreliable and unverified answers can waste time

Memory Bottleneck in Compile-time

In a study by Cahoon (2002) on compile-time analysis based on the programming language Java, he found that memory hierarchy in modern architecture is among the major performance bottlenecks in compile-time. However, when the software build and software compilation happens on the CI/CD pipeline rather than the software engineer's local development machine, the local development machine's performance does not matter anymore. It is acceptable for the software engineers to have a relatively weaker machine since the software is expected to be built and pass the automated tests on the remote CI/ CD pipeline. The CI/CD pipeline is the centralized location and the single source of to ensure the software build is fit for going into production. This means that improving the performance of the CI/CD pipeline will reduce the software build time for the software engineers, triggering a build in the pipeline. It shows that investing effort in optimizing the CI/CD pipeline is worthwhile.

Machine Learning Techniques for CI/CD Prediction

This research explored various machine learning (ML) techniques such as random forest (RF), XGBoost (XGB), gradient boosting (GB), k-nearest neighbor (KNN), support vector vegressor (SVR), which the characteristics and performance of the techniques are believed to be suitable in the CI/CD prediction's context. Kaliappan et al. (2021) have compared the performance of the above ML models in their study by evaluating them on the prediction of the COVID-19 reproduction rate. The research used common evaluation metrics such as mean absolute error (MAE), mean squared error (MSE), root mean squared error (RMSE), determination coefficient (R2), relative absolute error (RAE), and root relative

squared error (RRSE) to benchmark the performance of the ML model in regression task.The comparison result is shown in Table 2.

Table 2
Performance comparison between ML models in a Regression task

Performance Metrics	RF	XGB	GB	KNN	SVR
MAE	0.020	**0.019**	0.021	0.019	0.077
MSE	**0.001**	0.002	0.002	0.002	0.007
RMSE	**0.038**	0.041	0.041	0.041	0.085
R-Squared	**0.976**	0.973	0.973	0.973	0.884
RAE	0.106	**0.102**	0.112	0.102	0.404
RRSE	**0.154**	0.166	0.164	0.165	0.341

**Source:* Kaliappan et al. (2021)

As shown in Table 2, RF and XGBoost performed very well against the other ML models used in the study. RF achieved the best MSE, RMSE, R-Squared and RRSE, while XGBoost achieved the best MAE and RAE. RF and XGBoost are very popular ML models used in machine learning tasks. They are also ensemble ML methods that consider multiple ML models to produce a final prediction output that is generally more accurate than a single ML model.

Based on the analysis of Kaliappan et al.'s (2021) findings, RF and XGBoost are believed to be the ideal models to be used in the study because of their strong performance. Meanwhile, this study would also adopt other simple regression models, such as linear regression (LR) and support vector regression (SVR), to benchmark the performance with the two suggested ML models.

Related Work on Applying Machine Learning to DevOps Processes

The research conducted by Battina (2021) was identical to this research because it applied machine learning techniques to optimize the DevOps processes. Several machine learning techniques were studied to apply them to DevOps processes for better software quality. The author stated that dataset inputs, which are outputs from Git and Jenkins, can provide insight into the software delivery process. The anomalies of large code volumes and long build times in the data can be identified using machine learning models. The said study has a certain level of similarity to this research in the sense of performing prediction on software build time with a dataset of build event logs. This research brings confidence and proves the feasibility of delivering a solution that detects anomaly software build events in a CI/CD pipeline by comparing the instance with the prediction.

In another similar research, the authors proposed applying machine learning techniques to find defects in the CI/CD pipeline (Lazzarinetti et al., 2021). Attributes from software code version control include commits (author, commit message, date), changes in commit (added lines, deleted lines), and sonar measures (line of codes in the commit), which were used to identify the defects in the CI/CD pipeline. Albeit the slight difference in research methodology where the said research measures the software code version control attributes while this research uses attributes of the software build event on CI/CD pipeline, it shows there were prior efforts on experimenting with machine learning techniques on CI/CD pipelines with the same goal to improve the productivity of software engineers.

Related Work on Predicting Continuous Integration Build Failures with Evolutionary Search

Saidani et al. (2020) have conducted research to predict build failures on continuous integration by using evolutionary search. The research used a novel search-based approach based on multi-objective genetic programming (MOGP) instead of machine learning or deep learning. A model was built to predict whether the CI build will succeed or fail. The research was conducted with a benchmark of 56,019 builds from 10 large-scale software projects running on the Travis CI build system (Saidani et al., 2020). As a result, the author found that the method mentioned achieved a statistically better result than the models developed with machine learning techniques.

The main differences between the research conducted by Saidani et al. (2020) and this research are the features used and the prediction outcome. In the former, the researcher was trained on attributes specific to the files and codes changed in the commit, such as change size, file changes, and committer experience. In this research, the features used were the CI/CD pipeline attributes as well as the time when the commit is pushed to the pipeline. The target of the prediction is different as well. The former tries to predict whether the CI build will pass or fail, while this research predicts the time taken for the software build to complete in the CI/CD pipeline.

Literature Review Discussion

At the time of writing, no research papers and reports were found on the Internet or in research databases with the exact same objective: to predict the software build time on the CI/CD pipeline with machine learning. This research is considered relatively unique because it lacks other research to be benchmarked and compared against.

It is firmly believed that this research will be impactful and stir inspiration in the software development industry. Software engineers and technical leaders could benefit from their daily work of software development by applying the ML model to predict software build time on CI/CD pipeline and perform

data analysis to root cause CI/CD pipeline issues, ultimately bringing better productivity in software development. Without other research to compare with, this research should be conducted with a proper methodology and evaluated with correct judgment based on the research context and business requirements.

MATERIALS AND METHODS

Research Framework

Figure 2 shows the components of the research framework conducted in this research. The software development process could be illustrated in four areas: (1) development environment, (2) CI/CD Pipeline, (3) CI/CD prediction, and (4) production environment. The four areas are described in Table 3

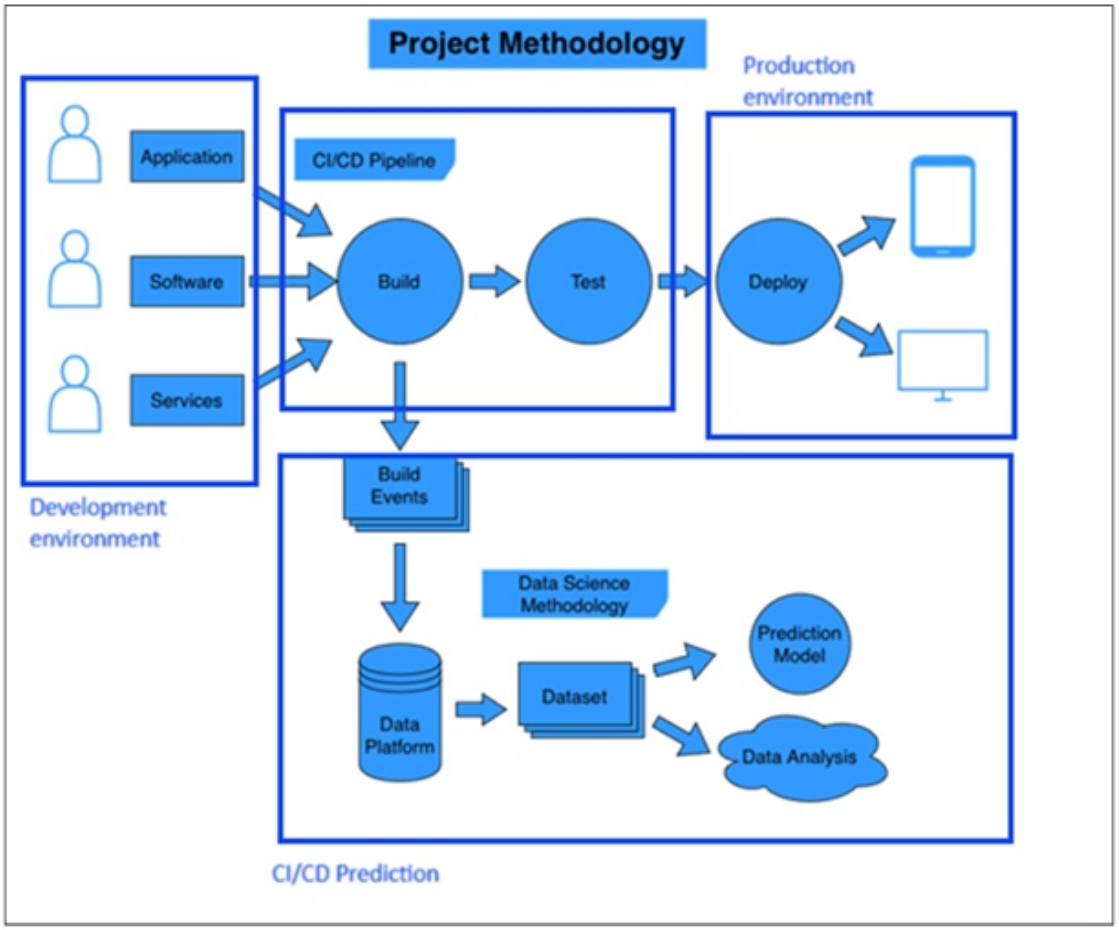

Figure 2. Research framework

Table 3
Description of research framework's components

Component	Description
Development environment	It is the environment where software engineers build applications and software codes locally. The finished codes will be pushed to the remote repository and version control system for further perusal.
CI/CD pipeline	It tracks the remote repositories and checks the status of new codes constantly "pushed." Auto build process will take place whenever new "commits" are available on the remote repository. Unit tests or integration tests come next after a successful build.
CI/CD prediction	The collected build event dataset is used to conduct software build time prediction using data science techniques.
Production environment	It is the environment where the successfully built and tested codes are deployed. New changes for the webpage can be rolled out immediately to the live environment. New web API services can be published to the production environment easily and efficiently with minimal to no server downtime.

Experiment Setting and Machine

Model selection and training were also solely conducted on the local machine, which performed very promisingly. The machine used is an Apple MacBook Pro 16 equipped with an Apple M1 Pro as the central processing unit (CPU) and 32GB of random access memory (RAM).

The biggest training dataset used in this project is around 800MB in CSV file form. The historical data was collected from a multi-national software development company. With the dataset loaded and preprocessed into Jupyter Notebook for model training, the machine handled the training without any hint of stress and completed the training within a few minutes. Considering the scale of the project's dataset, it is an acceptable performance for this project.

Research Methodology

This research adopted the cross-industry standard process for data mining (CRISP-DM), an industry-proven data science methodology, to organize data science projects. The sequence of the phases (Figure 3) may not be strict, and most projects may move back and forth between them when deemed necessary (IBM, 2021).

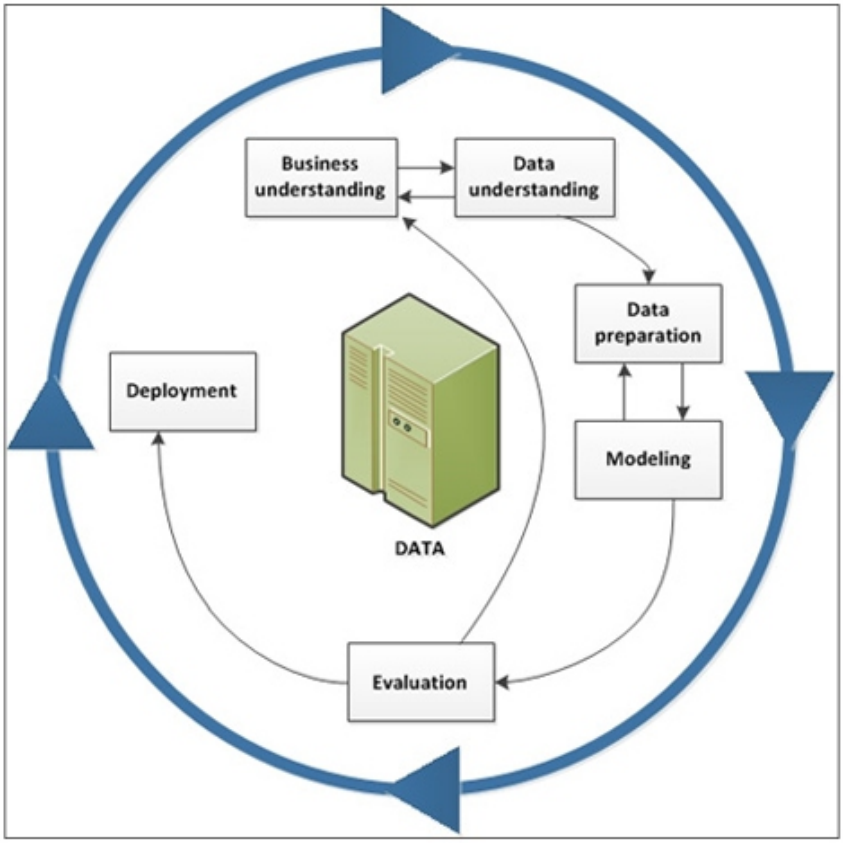

Figure 3. CRISP-DM methodology (IBM, 2021)

The first step in this research was to understand the business requirements and the available dataset. The Research acknowledges that the company's DevProd team was encountering inconsistent software build time on the CI/CD pipeline and would like to resolve this issue. The research has proposed adopting ML models, training the ML models with the build event dataset to predict CI/CD pipeline software build time, and further data analysis of the root causes of high software build time.

Next, the dataset needs to be prepared before the modeling step. Several steps, such as feature selection, feature encoding, and feature engineering, were performed to train the ML model.

With several ML models in mind, this research evaluated the ML models' performance on this preprocessed dataset. Mean squared error (MSE) was chosen as the evaluation metric because it is a common metric used to benchmark ML models in regression tasks. It averaged out the positive and negative differences by squaring the values. According to Hodson et al. (2021), mean squared error (MSE) is an ideal performance benchmark because of its link to the concept of cross-entropy from information theory. An ML model with a low MSE score is considered a good ML model, whereas a perfect ML model have a perfect score of 0 in MSE. After picking the best ML model, it will be tested with deployment. Depending on the scenario, the ML model might be tested on a test project to experiment with its performance and results. Further adjustments to the ML model and project setup can be made at this point.

Steps to Conduct Build Time Prediction with Data Science Techniques

Step 1: Feature Selection

Feature selection is the process of choosing the best features for the model under investigation (Rosidi, 2023). According to Rosidi (2023), correlated features that would cause multicollinearity and high computational power caused by too many features in a dataset were among the reasons why feature selection is crucial to a machine learning model. The original dataset is a CSV file generated by a Python script specifically written to preprocess the dataset file format exported by Splunk. The dataset has 79 columns. The required features are selected based on the domain expert's knowledge of the dataset. For example, it is logical to remove the feature git_commit_id since a Git commit ID that looks like "070dcfee" will not make any sense to the machine learning model since it is generated without bringing any meaning or significance other than uniquely identifying the specific Git commit. Many other features in the original dataset carrying unmeaningful values, such as randomized character strings, null values, and irrelevant values, were also removed because they would not provide useful information for model training. Finally, 13 columns (features) were selected as the prediction variables.

Step 2: Feature Encoding

Feature encoding is the step to transform features with string values, usually into numerical values comprehensible by machine learning models. It can be done manually by providing a mapping of values in the form of a data structure or by using data science libraries to automate the process when it comes to features with a high number of distinct values. Several feature encoding methods were used to transform the variables into the right format for the prediction process. A simple encoding process is adapted to store the mapping value for month and day, such as by declaring a Python Dictionary variable. In the case of features with a large number of unique values, label encoding was used to transform the relevant feature from categorical string labels into number labels by using the scikit-learn library method called LabelEncoder.

Step 3: Feature Engineering

The feature engineering technique creates useful features not in the original dataset and potentially improves the machine learning model's performance. In this case, the variable time_taken_min is created by calculating the time difference between existing features end_time and start_time to be this machine learning project's target variable (output). The new variable generated with feature engineering is added to the existing 13 variables chosen from the feature selection step to form 14 columns (features),

as shown in Figure 4, to be used as the prediction model's variables.

```
<class 'pandas.core.frame.DataFrame'>
Int64Index: 13325 entries, 5 to 70935
Data columns (total 14 columns):
 #   Column                Non-Null Count  Dtype
---  ------                --------------  -----
 0   date_hour             13325 non-null  int64
 1   date_mday             13325 non-null  int64
 2   date_minute           13325 non-null  int64
 3   date_month            13325 non-null  int64
 4   date_second           13325 non-null  int64
 5   date_wday             13325 non-null  int64
 6   date_year             13325 non-null  int64
 7   detail.build.state    13325 non-null  int64
 8   detail.job.exit_status 13325 non-null  float64
 9   detail.job.passed     13325 non-null  int64
 10  detail-type           13325 non-null  int64
 11  detail.pipeline.repo  13325 non-null  int64
 12  time_taken_min        13325 non-null  float64
 13  is_weekend            13325 non-null  int64
dtypes: float64(2), int64(12)
memory usage: 1.5 MB
```

Figure 4. A snippet of dataset columns after feature selection and engineering steps

Step 4: Identifying Relevant Machine Learning Models

According to the famous no-free-lunch theorem (NFL), the researchers cannot formally ground their conviction that some machine learning models are more sensible than others (Sterkenburg & Grünwald, 2021). Machine learning models have varying behaviors in different datasets, and the performance of the models is not guaranteed to be the same in all situations. Hence, there is a need to test the waters by trying out several models to find the most suitable model for this dataset.

The project first conducted experiments with simpler machine learning models such as linear regression (LR and support vector regression (SVR to get a glimpse into how these models would perform against the baseline benchmark. The experiments' results were unsatisfactory compared to the baseline benchmark.

Therefore, more complex machine learning models, such as RF, multilayer perceptron and XGBoost, were added to the experiment list to see if the complex model would achieve better performance than the simpler model. The results of each machinelearning experiment are shown in Table 4.

Table 4
Result of experiments with different machine learning models

Model Name	MSE
Baseline-dummy	299.36
Linear regression	293.50
Support vector regressor	308.49
Random forest	260.73
Multilayer perceptron regressor	278.91
XGBoost regressor	275.76

Table 4 shows that the more complex machine learning models, such as XGBoost regressor and multilayer perceptron regressor, have performed better than the baseline benchmark, linear regression, and support vector regressor by achieving lower MSE scores. However, they are less outstanding in comparison to the RF model because the model has achieved the best result with the lowest MSE score out of all models. As such, the RF model would be used to perform the software build time prediction.

RESULTS AND DISCUSSIONS

Experiment Set Up

The experiment was conducted with two datasets with different instances (Table 5) to explore whether the number of instances affects the prediction model's performance. Both datasets underwent the same data preprocessing methods and were trained using the same machine learning, the random forest (RF) model. For a small dataset, 70% of the data was used for training, while the other 30% was used for testing. The dataset is retrieved from Splunk with 1 week's worth of data for the build event dataset. As for the big dataset, 5-fold cross-validation was used to validate the model. The dataset was retrieved from AWS CloudWatch, which had 1 month's worth of data for the build event dataset. number of features used in the big dataset was reduced to 8 from 14 in the small dataset by removing irrelevant features that scored zero in feature importance, deduced from the RF model trained on the small dataset.

Table 5
Comparison of small and large datasets

Dataset	Small Dataset	Big Dataset
Size of data frame	2394	44344
Number of features	14	8
Number of instances	171	5543

The prediction of software build time on the CI/CD pipeline was made using the trained RF model to perform prediction on a new data instance.

For example, the trained RF model will give a new data instance with the same set of features. Since the RF model was trained on the dataset with the same set of features, it will be able to provide a prediction for the new data instance after "learning" from the training dataset.

Table 6 shows the result of the software build prediction with an RF model with small and big datasets. The RF model's performance in the smaller dataset is highly assuring and outperformed by the dummy regressor, which is used as the baseline for comparison in this experiment. On the other hand, the RF model with a big dataset did not outperform the baseline dummy regressor too much (less than 1.0) as previously expected.

Table 6
Prediction result comparison for small and big datasets

Dataset	Model	MSE	RMSE
Small dataset	Dummy regressor	53.232	7.296
	RF model	14.306	3.782
Big dataset	Dummy regressor	19.008	4.360
	RF model	16.642	4.079

Discussion on Result

The experiment showed that the RF model performed better when using a small dataset than a big dataset. There could be several possible reasons for the not-so-good performance of a big dataset. Firstly, the dataset might have a high variance. Secondly, the dataset might be imbalanced. Thirdly, more features could be required for the big dataset to produce more accurate prediction output. Fourthly, the repository that was used might have glitches in the build time in the dataset.

Considering the outstanding performance of the RF model over the dummy regressor in the small dataset, it is believed that the result of the RF model that was trained in this research was significant. With the RMSE score of 3.782 achieved in the small dataset, where the feature unit is in minutes, the model's prediction is only 3.782 minutes away from the actual result on average. In a dataset with software build,

events take 20 minutes to 1 hour. The RMSE score of 3.782 achieved by the RF model is considered outstanding in this business context.

While it is fine to conduct software build time prediction with a small dataset at a time by using a dataset with build data for a shorter period, with the latest trend analysis, the RF model is the ideal machine learning model to be used on this software build dataset for software build time prediction.

Direct comparison of this research with other existing research is unavailable because this research is unique as far as the researchers' best effort of literature search. However, it is important to note that the result achieved by the RF model is reassuring and gives confidence in the technique of applying ML models to predict CI/CD pipeline software build time and provide further analysis using the model trained to give better suggestions on root cause leading to slow CI/CD pipeline performance, in comparison to using the traditional and unstructured methods as discussed in Table 1.

Impact of Research in the Real World

The RF model has been deployed in a small-scale project's CI/CD pipeline for testing and observing its performance. After deploying the model on the testing project's CI/CD pipeline, the team has observed a similar performance of MSE score with the RF model trained. The RF model is able to predict software build time on the CI/CD pipeline, which is relatively close to the actual software build time on the pipeline.

Due to the limited scope of the test environment and dataset involved, the major factor that affects the software build time on the CI/CD pipeline the most is the start time. It seems that in this environment and scope, the start time, especially the hour it started, will impact the most on how much time it will take to finish the software build on the CI/CD pipeline. This is explainable because although software building might happen frequently within a certain hour, the busy CI/CD pipeline might not have enough agents and hardware resources to perform the software build requests in a timely manner. Ultimately, this leads to a longer waiting time and, thus, a longer software building time.

It is hoped that this research will inspire software engineers, CI/CD engineers and technical leaders to adopt ML techniques into their infrastructure and technology stack. This will improve software development productivity by providing accurate software build completion time. It will also decrease CI/CD pipeline downtime coupled with performance improvement with the help of data analysis and machine learning techniques to debug issues.

Adopting the technique proposed in this research will save time and provide a higher accuracy of troubleshooting on the CI/CD pipeline. These will all lead to a lesser downtime of CI/CD pipelines with higher performance. Engineers will also better understand the factors leading to depriving performance of the CI/CD pipeline. The monetary costs of the computing infrastructures will be saved for the above-

mentioned reasons. Faster software shipping speed thanks to the efficient CI/CD pipeline enables speedy business software delivery. A healthy and efficient CI/CD pipeline would improve the recovery crisis of website downtime.

CONCLUSION

This research explored the machine learning model to predict software build time with various sizes of datasets. Five machine learning models, linear regression, support vector regressor, random forest, multilayer perceptron regressor, and XGBoost regressor, were experimented with to find the best prediction model to predict software build time with the selected 14 features. The experiment showed that the RF model with a small dataset in this research experiment is the best model for software build time prediction.

Without prior research on this specific subject matter, this research has uniquely provided an approach to adopting data science and ML techniques in the CI/CD pipeline to predict the software build time-based on a dataset of past software build events. Data analysis could be done with the help of the trained model to further analyze and debug the performance issues in the CI/CD pipelines.

In an ideal world, developers would not only wish to reduce their software build time optimally but also get an accurate prediction of their software build time. It enables the developers to perform at a higher level of productivity and brings more satisfaction to their daily jobs. This brings us to the goal of this research: discovering the feasibility of applying machine learning and data analysis to help predict the software build time, as well as discovering major factors that could lead to better-optimized software build time.

FUTURE WORK

The first possible improvement that came to mind was introducing more features to the dataset. The project dataset did not have several good candidates for features such as agent (a virtual agent that runs jobs), waiting time, and instance startup time (time for virtual machines to boot into usable state). They would certainly bring more information and insight into the study and help better analyze how other factors could also contribute to a higher build time. By taking more meaningful dataset features into account, bottlenecks can be identified to help bring improvement for a faster build time. The machine learning model also gains robustness with more relevant features in the training dataset.

Another future work that would take the project idea to a further step is to train a generalized machine learning model. The RF model was trained in very specific variables in the current project. Only one single code repository and specific CI/CD pipeline configuration were included in this project dataset.

The model is expected to not perform well universally outside the specific features or variables it was trained on. The ideal machine learning model should have the ability to cater to changes, such as predicting across different code repositories and adding extra steps into the CI/CD pipeline. These are indeed ambitious targets for the project and require an immense amount of expert knowledge with a deep understanding of the domain. An enormous amount of data collection, analysis and research into the CI/CD pipeline is required to deliver this seemingly bold yet highly rewarding improvement.

ACKNOWLEDGEMENT

The authors thank Universiti Sains Malaysia for funding this paper's publication.

REFERENCES

Amazon Web Services. (2023). Practicing continuous integration and continuous delivery on AWS. AWS. https://docs.aws.amazon.com/pdfs/whitepapers/latest/practicing-continuous-integration-continuous delivery/practicing-continuous-integration-continuous-delivery.pdf

Battina, D. S. (2021). The challenges and mitigation strategies of using devops during software development. International Journal of Creative Research Thoughts (IJCRT), 9(1), 4760–4765.

Bedrina, O. (2023, August 7). Best continuous integration tools for 2023 – Survey results. JetBrains Blog. https://blog.jetbrains.com/teamcity/2023/07/best-ci-tools/

Cahoon, B. D. (2002). Effective compile-time analysis for data prefetching in Java [Doctoral dissertation, University of Massachusetts Amherst]. University of Massachusetts Amherst. https://www.cs.utexas.edu/ users/mckinley/papers/cahoon-thesis.pdf

Fairbanks, J., Tharigonda, A., & Eisty, N. U. (2023, May 23-25). Analyzing the effects of CI/CD on open source repositories in github and gitlab. [Paper presentation]. IEEE/ACIS 21st International Conference on Software Engineering Research, Management and Applications (SERA), Orlando, Florida. https:// doi.org/10.1109/sera57763.2023.10197778

Hodson, T. O., Over, T. M., & Foks, S. S. (2021). Mean squared error, deconstructed. Journal of Advances in Modeling Earth Systems, 13(12), Article e2021MS002681. https://doi.org/10.1029/2021ms002681 IBM. (2021, August 17). CRISP-DM help overview. IBM. https://www.ibm.com/docs/en/spss-modeler/ saas?topic=dm-crisp-help-overview

Jaspan, C., & Green, C. (2023). developer productivity for humans, part 4: Build latency, predictability, and developer productivity. IEEE Software, 40(4), 25–29. https://doi.org/10.1109/ms.2023.3275268

Kaliappan, J., Srinivasan, K., Mian Qaisar, S., Sundararajan, K., Chang, C. Y., & C, S. (2021). Performance evaluation of regression models for the prediction of the COVID-19 reproduction rate.

Frontiers in Public Health, 9, Article 729795. https://doi.org/10.3389/fpubh.2021.729795

Lazzarinetti, G., Massarenti, N., Sgrò, F., & Salafia, A. (2021, November 30). A machine learning based framework for continuous defect prediction in CI/CD pipelines. [Paper presentation]. Proceedings of the Italian Workshop on Artificial Intelligence and Applications for Business and Industries (AIABI), Milan, Italy.

Red Hat. (2023, December 12). What is CI/CD?. Red Hat. https://www.redhat.com/en/topics/devops/whatis-ci-cd

Rosidi, N. (2023, June 6). Advanced feature selection techniques for machine learning models. KDnuggets. https://www.kdnuggets.com/2023/06/advanced-feature-selection-techniques-machine-learning-models. html

Saidani, I., Ouni, A., Chouchen, M., & Mkaouer, M. W. (2020). Predicting continuous integration build failures using evolutionary search. Information and Software Technology, 128, Article 106392. https:// doi.org/10.1016/j.infsof.2020.106392

Silverthorne, V. (2022, February 15). 10 Reasons why your business needs CI/CD. GitLab. https://about.gitlab. com/blog/2022/02/15/ten-reasons-why-your-business-needs-ci-cd/

Snyk. (2020, October 1). What is CI/CD? CI/CD Pipeline and Tools Explained. Snyk. https://snyk.io/learn/ what-is-ci-cd-pipeline-and-tools-explained/

Sterkenburg, T. F., & Grünwald, P. D. (2021). The no-free-lunch theorems of supervised learning. Synthese, 199(3), 9979–10015. https://doi.org/10.1007/s11229-021-03233-1

ISSN 0128-7680

A Novel Approach to Evaluating HEMA Polymer Gel Dosimeters Using Molecular Vibrational Features

Muhammad Alhassan1,2*, Azhar Abdul Rahman1, Iskandar Shahrim Mustafa1, Mohd Zahri Abdul Aziz3, Mohd Zakir Kassim 3, Mohammed Salem Abdullah Bagahezel3, Habib Ahmad Ibrahim1 and Kabiru Alhaji Bala1

1School of Physics, Universiti Sains Malaysia, Main Campus, Pulau Pinang, Malaysia
2Department of Physics, Federal University Dutsin-Ma, 821101 Katsina State, Nigeria
3Department of Biomedical Imaging, Advanced Medical and Dental Institute, Universiti Sains Malaysia, Bandar Putra Bertam, 13200 Kepala Batas, Pulau Pinang, Malaysia

ABSTRACT

A polymer Gel Dosimeter (PGD) provides essential three-dimensional (3D) radiation dose distribution for the radiotherapy planning system (TPS). This study investigates the use of infrared absorption spectrum as a novel and more cost-effective alternative to Magnetic Resonance Imaging (MRI), Nuclear Magnetic Resonance (NMR), and Optical Computed Tomography (Optical CT) for reading out PGDs. The PGDs were fabricated using 2-Hydroxyethyl methacrylate (HEMA), maltose, N'N, methylene(bis)acrylamide (Bis), gelatin, deionized water (DI Water), and Tetrakis (hydroxymethyl) phosphonium chloride (THPC), and were irradiated using a Linear Accelerator (LINAC) within the range of 0–30 Gy. The possibility of translating molecular vibrational frequency, amplitude, and energy of vibration into absorbed dose was explored by analyzing the absorption spectra in the near-infrared region (NIR) with wavelengths between 750–1100 nm. The findings reveal that these vibrational properties can be employed to interpret irradiated PGDs. Furthermore, an increase in maltose concentration within the 0–520 mM range widens the linear dose range and enhances sensitivity. The PGDs exhibit temporal stability up to 7 days irradiation, and the span of their response remains relatively unaffected by scanning temperature. In conclusion, NIR spectroscopy offers a cost-effective method for interpreting PGDs, potentially improving the affordability and efficiency of PGD dosimetry in clinical radiotherapy. This holds particularly promising for less developed countries, aligning with the sustainable development goal (SDG) of ensuring affordable healthcare for all. We finally recommend further research into translating the molecular vibrational parameters into 3D images.

Keywords: *HEMA, infrared absorption spectrum, maltose additive, polymer gel dosimeter, saccharide additive*

INTRODUCTION

Radiotherapy is a medical technique involving collective responsibilities among radiation oncologists, medical physicists, radiographers, and radiation technologists to eliminate cancerous cells in the human body using ionizing radiation. It becomes increasingly crucial with rising cancer incidences (Jaszczak et

al., 2020). There are two common types of radiotherapy: internal radiotherapy or brachytherapy, which involves placing sealed radioisotopes near or inside the tumor (Shukor et al., 2022), and external beam radiotherapy, irradiating the tumor from outside the body. Precision in dosage prescription is paramount in radiotherapy, necessitating careful planning to ensure the target volume receives the proper dose without harming surrounding healthy tissues. As such, the need for a tool that could measure the dose distribution in a 3D manner arises (Kozicki et al., 2020). PGD is a tool made from hydrogels such as gelatin within which monomer is uniformly distributed and readily polymerizes on irradiation and is proven capable of measuring complex 3D radiation dose distribution with high precision and spatial resolution (Adliene et al., 2020; Jaszczak et al., 2020; Rabaeh et al., 2021; Shih et al., 2022).

On irradiation, radiation-induced polymerization occurs as a function of the absorbed dose in such a way that the level of polymerization could thereafter be translated into the absorbed dose (Mustaqim et al., 2020; Shih et al., 2022). Various physical and chemical changes in PGDs – such as shifts in transverse relaxation rate (R_2) during MRI, relaxation times during NMR, and optical appearances via optical CT scanning (OCS) could be translated into absorbed dose (Adliene et al., 2020; Jaszczak et al., 2020), alongside UVvisible spectrophotometry (UV-Vis) revealing optical changes and electronic transitions (Ishak et al., 2015), changes in CT number in x-ray CT scanning (Javaheri et al., 2020), and changes in speed of sound during Ultrasound scanning (Javaheri et al., 2020). Recent advancements utilize angular modulation, plasmonic sensors, and reflection intensity changes during Polarization-Sensitive Optical Coherence Tomography (PS-OCT) for evaluating polymerization (Adliene et al., 2020; Shih et al., 2022), with future predictions involving electrical impedance tomography (EIT), photoacoustic, and diffuse optical tomography (DOT) for PGD readouts (Deene, 2022). However, these techniques often rely on specialized machinery, posing obstacles to the realization of the sustainable development goal of providing comprehensive healthcare, especially in less developed countries.

Our present work pioneers translating molecular vibration-related changes in near infrared (NIR) absorption spectra into absorbed doses. The advantages of NIR spectroscopy are the availability of infrared (IR) Spectrophotometer or Vis-IR spectrophotometer in laboratories for identification of chemical substances, it is non-destructive, and is a fast technique compared to others (Masithoh et al., 2023; Zapata et al., 2021) and nowadays, some manufacturers such as Shimadzu, Japan manufactures UV-Vis spectrophotometers with extended energy range to NIR region and could be used to obtain absorption spectra and transmittance spectra of a sample within 200-1100 nm wavelength range. The utilization of UV-Vis spectrophotometer for PGD readout could be considered a better option due to its availability and cost-effectiveness (Lotfy et al., 2017).

The use of IR as a PGD readout technique hinges on the fact that irradiation-induced polymerization and crosslinking within the PGD lead to changes in molecular bonds (Deene, 2022), subsequently

influencing the spectral position, bandwidth, and peak. These changes signify modifications in molecular vibration amplitude, frequency, and energy.

When a PGD is exposed to electromagnetic radiation (e.m. waves), three types of interactions can occur: (1) changes in rotational energy levels of molecules (this requires the least energy, typically at longer wavelengths), (2) changes in (this requires moderate energy, often happening in the NIR, and (3) electronic transitions (this requires the most energy, occurring at ultraviolet or visible wavelengths). While NIR is primarily associated with vibrational spectroscopy, it can also encompass electronic and rotational spectroscopies (Ozaki, 2021; Zapata et al., 2021). The spectral bands observed in the NIR are mostly due to functional groups containing hydrogen atoms, such as OH, CH, and NH, which are also present in this study's constituents of the PGDs.

In existing literature, IR spectrophotometers are employed in chemistry, biochemistry, biology, and material sciences to obtain transmittance or reflectance spectra within the 780–2500 nm range. These spectra are then translated into molecular vibrations for qualitative and quantitative analyses, determining the presence or concentration of specific materials, bonds, or functional groups in a sample (Darwish & Darwish, 2022; Pratiwi et al., 2022; Renner & Fritz, 2020; Zapata et al., 2021).

The scope of this study is limited to evaluating radiation-induced changes linked to molecular vibrations in the PGDs. Consequently, a single prominent absorption band within the NIR range is chosen to establish a connection between molecular vibrational changes and the absorbed dose that causes these changes. The limitation of this work the usage of NIR for dose evaluation is the limited penetrability of IR, which might restrict its application in large PGD phantoms.

Also, the shapes and sizes of sample holders in the present UV-Vis-IR spectrophotometers might restrict the evaluation of PGDs in humanoid phantoms. This study aims to produce PGD using the less toxic monomer HEMA with a maltose additive. Subsequently, these PGDs will be irradiated with X-rays from a LINAC, and the vibrational parameters will be translated into absorbed doses.

MATERIALS AND METHOD

Gel Preparation

Four PGDs with varying maltose concentrations were prepared using the following components: DI Water (89.0%), gelatin (Type B, 225 g bloom) (6.0%), HEMA (2.7%), Bis (2.0%), and THPC (0.2%). All reagents except DI Water were obtained from Sigma-Aldrich, Germany. DI water was produced in the lab using the Arium® Pro water system machine.

The PGDs were prepared under normal atmospheric (normaxic) conditions (Nezhad et al., 2021).

Throughout the PGDs' preparation, a hot plate with an integrated magnetic bar stirrer was used to facilitate the heating and stirring of the mixture. The PGDs were prepared by first heating DI water to 48°C to enable full dissolution of Bis. Following the addition of Bis, gelatin was added. The heating knob was switched off while the stirring continued to allow the mixture to cool. When the mixture became clear and transparent and cooled to 35°C, maltose was added, followed by HEMA and THPC at 27°C to avoid premature polymerization. The sequential addition of the components and the corresponding temperatures are outlined in Figure 1

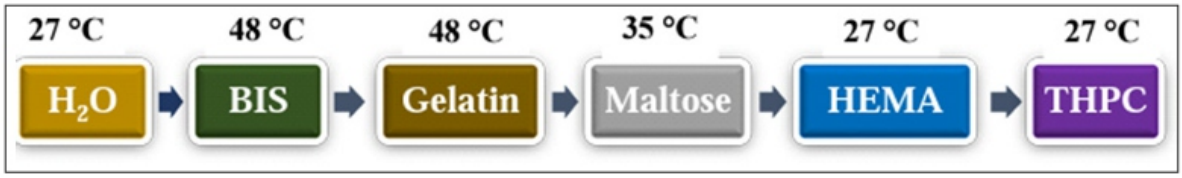

Figure 1. Preparation of PGD with the Sequential addition of its components

Following the addition of the last component, the PGDs' formulation was stirred for over 15 minutes at room temperature to ensure uniformity within the gel matrix. The mixture was then transferred to 4.5 cm^3 Perspex cuvettes with a 1.0 cm path length, tightly sealed with parafilm to prevent oxygen penetration, and placed in a refrigerator maintained at 4-6°C for gelation. These dosimeters are named here 'HEMAMAL' as an acronym
for 'HEMA dosimeter + MALTOSE'; they are labeled as HEMAMAL1, HEMAMAL2, HEMAMAL3, and HEMAMAL4, corresponding to maltose concentrations of 0 mM, 80 mM, 230 mM, and 520 mM, respectively.

Irradiation

The PGDs were irradiated on the third day after manufacturing using an Elekta LINAC with a photon energy of 6 MV. The samples were positioned on a water phantom 5 cm thick and beneath another water phantom 1.5 cm thick, maintaining a source-surface distance (SSD) of 100 cm. This setup was within a 10 × 10 cm^2 field of view (FoV) in the isocenter. As mentioned elsewhere, the water phantom ensures uniform radiation distribution among the PGDs, facilitates radiation build-up effects, and maintains scattering conditions (Aljarrah et al., 2016).

The four batches of the PGD were irradiated to 5, 10, 15, 20, 25, and 30 Gy, while one PGD from each batch was left unirradiated (control sample). The arrangement for sample irradiation is illustrated in Figure 2

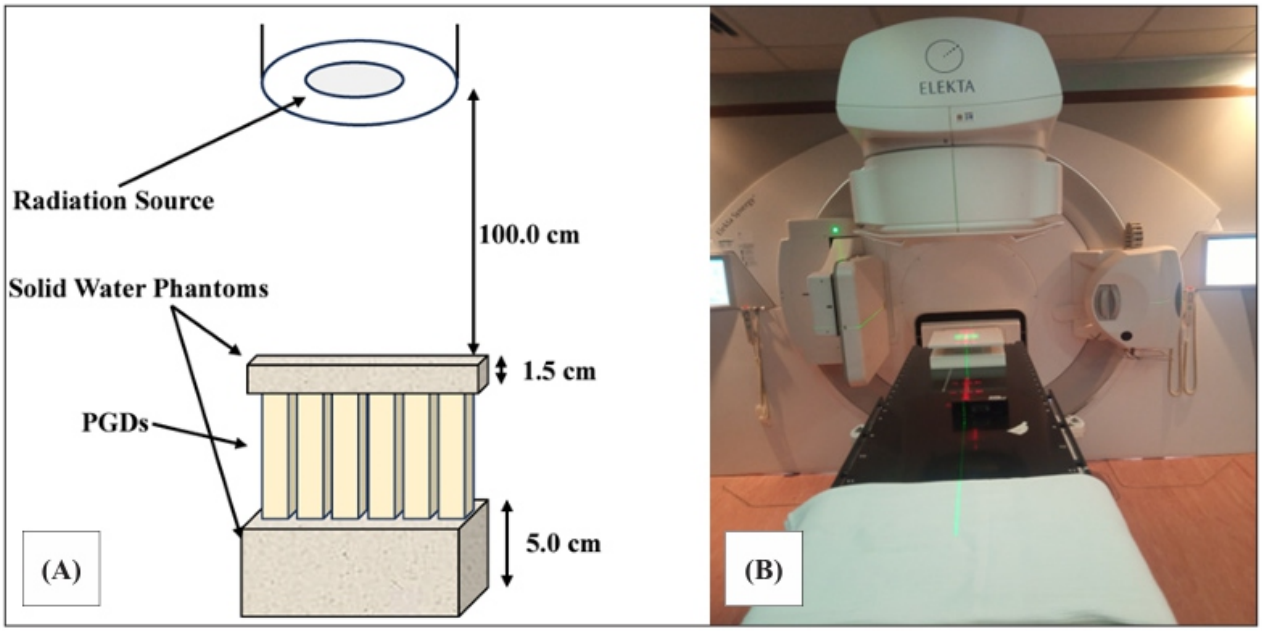

Figure 2. The visualization of irradiation setup with (A) The schematic diagram of the irradiation procedure and (B) Placement of PGDs at the isocenter of radiation FoV with the help of a laser beam

Dose Readout

The Shimadzu UV-1800 is a UV-Vis Spectrophotometer designed to scan samples across ultraviolet (UV), visible (Vis), and certain IR wavelengths. It can provide both absorption and transmittance spectra. Prior to the scanning process, the machine was allowed to warm up and complete initializations. Subsequently, it was configured for absorbance mode within the wavelength range of 750–1100 nm, a portion of the NIR spectrum (Ozaki, 2021). The scanning interval was set to be 1 nm at a medium scan speed, and the range of absorbance was 0.00–4.00. A Perspex cuvette almost full of DI water was used as the reference sample, and baseline correction was performed. The PGDs were scanned while maintaining the room temperature at 22.0 ± 0.5°C with the help of an air-conditioning system while the doors and windows remained closed.

In this study, we employed three principles to translate molecular vibrations into absorbed doses.

1. Relationship between Vibrational Amplitude and Concentration: This principle is rooted in Beer Lambert's law, which states the direct proportion between absorbance and concentration of the measured component (Equation 1)

$$A = \varepsilon l c \qquad [1]$$

Where A represents peak absorbance or band intensity/amplitude, ε is the absorptivity, l is the optical path length, and c is the concentration (Darwish & Darwish, 2022; Pratiwi et al., 2022). In our case, concentration signifies polymerization levels and reflects the absorbed dose. Accordingly, we plotted graphs depicting changes in absorbance (ΔA) and peak absorbance (Ap) against absorbed dose.

2. Relationship between Absorbed Energy and Spectral Bandwidth: Heightened polymerization necessitates greater energy to induce molecular vibrations from lower to higher energy states. This results from structural changes, viscosity changes, and changes in molecular conformity (Darwish & Darwish, 2022; Deene, 2004; Ishak et al., 2015). Energy and vibrational frequency are correlated through Equation 2:

$$E = h\nu \qquad [2]$$

Where E is quantized energy, h is Planck's constant, and is the frequency (AbdelGhany et al., 2020; Ishak et al., 2015). If absorbed energy ΔE leads to an electronic transition or sets molecules into vibration, Equation 2 can be expanded to relate the energy to the absorbance bandwidth, as shown in Equation 3

$$\Delta E = h\left(\nu_f - \nu_i\right) = hc\left(\frac{\Delta\lambda}{\lambda_f \lambda_i}\right) \qquad [3]$$

Where $\nu_i = \frac{c}{\lambda_i}$ and $\nu_f = \frac{c}{\lambda_f}$ are initial and final vibrational frequencies before and after energy absorption, and Δλ is the bandwidth or the difference between λ_i and λ_f in cm. We plotted bandwidth against absorbed dose to capture this relationship.

Relationship between Energy and Molecular Frequency/Wave Number:
Equations 2 and 3 establish energy, vibration frequency, and wavelength connections. At λ_{max}, energy aligns with wave number ($\tilde{\nu}$) as shown in Equation 4:

$$E = hc\tilde{\nu} \qquad [4]$$

Where $\tilde{\nu} = \frac{1}{\lambda_{max}}$ is the wave number and is measured in cm^{-1}.

Equation 5 defines the wave number for a harmonic oscillator, which is connected to the force constant of the molecular bonds and reduced mass.

$$\tilde{\nu} = \frac{1}{2\pi}\sqrt{\frac{k}{\mu}} \qquad [5]$$

Where k represents the force constant in Ncm^{-1}, and μ is reduced mass in kg (Darwish & Darwish, 2022; Ozaki, 2021). In our case, varying polymerization levels and crosslinking lead to different concentrations of double bonds and functional groups within the irradiated polymer matrix. Consequently, different k and μ values emerge. Functional groups were also noted to influence PGD sensitivity to radiation (Deene, 2004). We plotted wavenumbers against absorbed dose to reflect this connection.

RESULT AND DISCUSSION

Absorption Spectra

The irradiated PGDs were scanned using a UV-Vis-IR spectrophotometer capable of covering a portion of the NIR spectrum. The dose evaluation was based on absorption spectra within the 750–1100 nm range, which are depicted in Figure 3.

The absorption spectra in Figure 3 (A)-(E) reveal distinct peak positions (λ_{max}) among the four PGDs. It is attributed to the influence of the maltose additive. This λ_{max} shift is also evident within each batch of PGDs irradiated at varying energies. This intra-batch shift is attributed to differing levels of polymerization and crosslinking, which impact molecular bond vibrations and can be correlated with absorbed doses causing polymerization and crosslinking. Figure 3(E), with an expanded view in 3(F), illustrates bandwidths of absorption spectra for HEMAMAL4 PGDs irradiated at 5, 10, 15, 20, 25, and 30 Gy doses. Bandwidths are measured at half peak absorbance ($\frac{1}{2}A_p$) for each spectrum. The accompanying table in Figure 3(F) indicates that bandwidth increases with an increase in absorbed dose.

Results in Figure 3(A)-(E) reveal the presence of multiple absorption bands with varying heights and widths attributed to diverse functional groups like OH, CH, and NH in dosimeter constituent components (Ozaki, 2021). These findings align with our expectation of λ_{max} shifting to higher energy (shorter wavelength) due to increased concentration of specific components, consistent with Beer Lambert's Law (Equation 1). These observations indicate the effect of absorbed dose on parameters associated with spectral height and width (Darwish & Darwish, 2022).

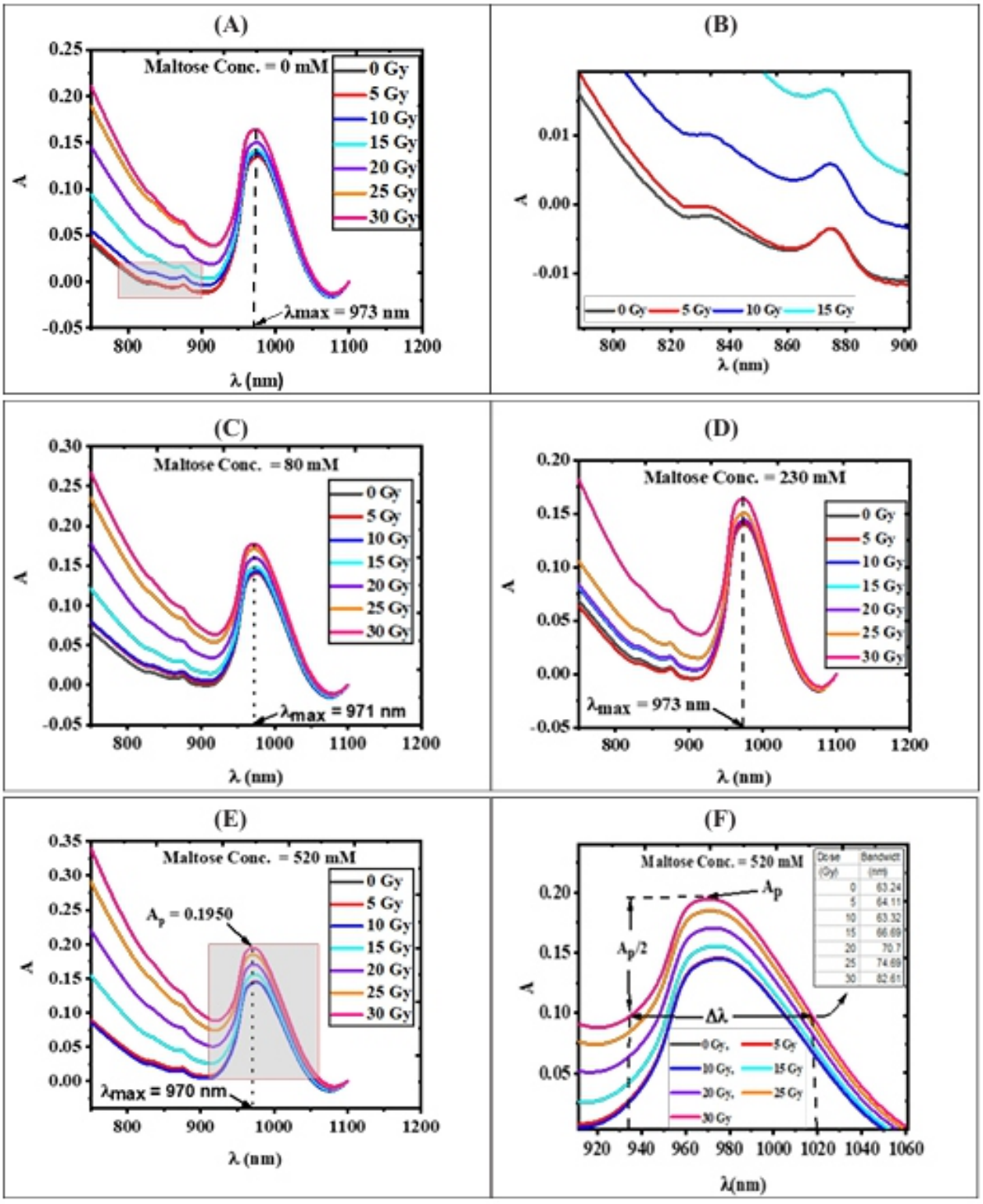

Figure 3. The absorption spectra of four PGDs (A) HEMAMAL1, (B) an enlarged portion of (A) as indicated by the arrow, (C) HEMAMAL2, (D) HEMAMAL3, (E) HEMAMAL4, and (F) an enlarged portion of (E) showing the bandwidth of HEMAMAL4, irradiated to 0-30 Gy

Dose-response

The dose-response, represented by (1) change in absorbance (ΔA), (2) peak absorbance (Ap), (3) bandwidth (Δλ), and (4) wave number ( ), was plotted against the absorbed dose. The resulting graphs are displayed in Figure 4.

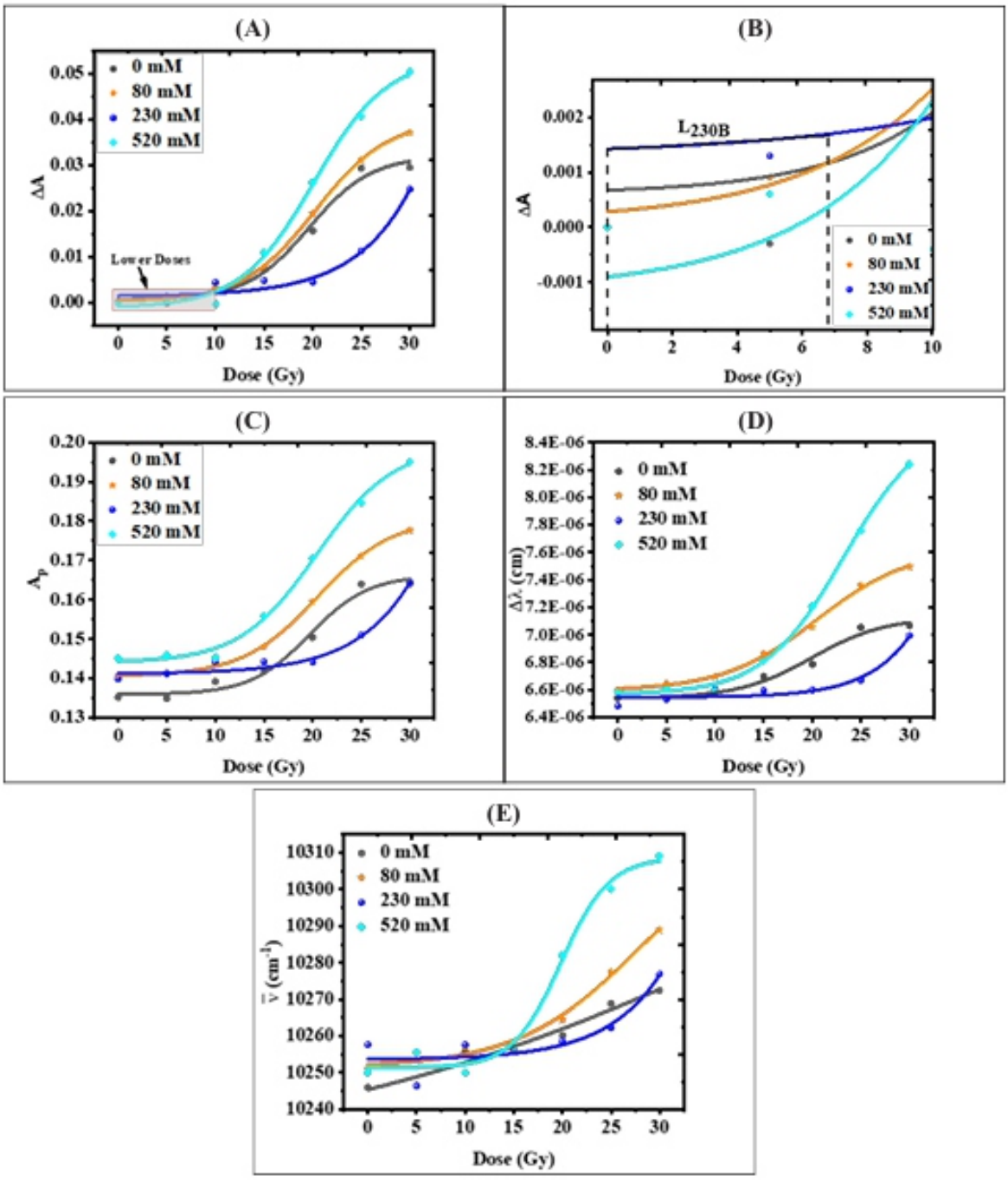

Figure 4. The relationship between the absorbed dose and the measured responses is (A) change in absorbance, (C) peak absorbance, (D) bandwidth, and (E) wave number. (B) is an enlarged portion of the lower dose region shown in (A)

The curves in Figure 4 (A)–(E) depict dose-response patterns for the four PGDs under investigation. These curves were fitted to sigmoidal dose-response curves and can be described mathematically using Hill's Equation, represented by Equation 6.

$$y = A_1 + \frac{A_1 + A_2}{1 + 10^{(Log_x 0 - x)p}} \quad [6]$$

In this equation, y represents the measured response, x represents the dose, A1 and A2 denote the lower and upper response limits, and p indicates the slope measured at the steepest point ($x = \log_x 0$, and $y = \frac{A_1 + A_2}{2}$) (Gadagkar & Call, 2015).

The findings in Figure 4(A)–(E) demonstrate gradual response increments at lower doses, followed by more substantial and linear increments at higher doses. As the dose approaches 30 Gy, the response tends to slow again. These graphs highlight that the lower dose range, the extent of the linear region, and the point where responses slow down a second time vary with the response type and the amount of maltose present in each dosimeter. For instance, the linear dose ranges for HEMAMAL1, HEMAMAL2, HEMAMAL3, and HEMAMAL4 are approximately 14.80–24.60 Gy, 14.20–25.70 Gy, 27.00–30.00 Gy, and 14.20 Gy–25.80 Gy, respectively. Comprehensive ranges for all PGDs based on the four different response types used in this study, along with the coefficient (R^2) for each, are presented in Table 1.

The nonlinearity observed in the response of PGDs at lower doses compared to higher doses is attributed to a mechanism that remains not fully understood (Adliene et al., 2020). However, it is suggested that inhibitors such as oxygen could form peroxide which can potentially terminate the polymerization reaction at lower doses. In contrast, the polymerizing system has a higher viscosity at higher doses, facilitating interactions between growing polymer chains. This impedes termination by inhibitors and results in a steeper response (Deene, 2004). Nevertheless, linearity can still be achieved at lower doses, as illustrated in Figure 4(A), the magnified section in 4(B), and 4(C)–(D), where HEMAMAL3 exhibits linear dose-response within the 0-6 Gy range. However, the gradient is comparatively lower than at higher doses (Deene, 2004).

Similar cases to this observation have been documented in the literature. For the Fricke-xylenol orange (FXO) gel dosimeter, evaluated using Optical CT, linearity within the 1–8 Gy range and becomes sublinear for doses below or above this interval (Nezhad & Geraily, 2022). BANG PGD, as manufactured by Farajollahi et al. (1999), also demonstrates a linear region up to 10 Gy (Nezhad & Geraily, 2022). In our study, the linear regions of the dosimeters start from doses around 13.6 Gy, with varying ranges of linearity spanning 2.7–30 Gy, as detailed in Table 1. This variation arises from differences in maltose content within each PGD and the specific response type being measured. Such

observations are unsurprising, as reported linear dose ranges in existing literature are dependent upon PGD's composition, irradiation techniques, and scanning techniques. For example, the PAMPSGAT PGD prepared from 2-Acrylamido2-MethylPropane Sulfonic acid (AMPS), and scanned via MRI, exhibits a linear dose range within 10–40 Gy (Rashidi et al., 2020). Similarly, NIBMAGAT, synthesized from N-(Isobutoxymethyl) acrylamide monomer and evaluated through UV-Vis readout and NMR, demonstrates linearity within 5–20 Gy, with a linear range of 15 Gy (Lotfy et al., 2017). VIPAR dosimeter, evaluated by Kipouros et al. (2001), is reported to maintain linearity up to 40 Gy (Nezhad & Geraily, 2022).

Table 1
The linearity and correlation coefficients of fitting to the sigmoidal dose-response curve of the four PGDs under study, with different types of responses, are shown

Type of Response	Maltose Conc. (mM)	D_1 (Gy)	D_2 (Gy)	Linearity (Gy)	R^2
ΔA	0	14.80	24.60	9.80	0.9840
	80	14.20	25.70	11.50	0.9997
	230	27.00	30.00	3.00	0.9792
	520	14.20	25.80	11.60	0.9957
A_p	0	15.20	24.20	9.00	0.9834
	80	15.30	25.70	10.40	1.0000
	230	25.70	30.00	4.30	0.9817
	520	14.70	26.00	11.30	0.9964
Δλ	0	14.20	26.70	12.50	0.9792
	80	13.60	27.80	14.20	0.9953
	230	27.00	30.00	3.00	0.9489
	520	17.30	28.10	10.80	0.9840
$\tilde{\nu}$	0	0.00	30.00	30.00	0.9643
	80	19.30	30.00	10.70	0.9920
	230	27.30	30.00	2.70	0.8253
	520	16.00	24.10	8.40	0.9616

D_1 = beginning of the linear dose region, D_2 = end of the linear dose region, and R^2 = correlation coefficient

Unlike other PGDs, HEMAMAL1, depicted in Figure 4(E), demonstrates fitting to both sigmoidal dose-response curve ($R^2 = 0.9643$) and linear curve ($R^2 = 0.9578$) within the 0–30 Gy range, based on changes in bandwidth. It displays a gradient of 0.9152 $cmGy^{-1}$. Similarly, the VIPET dosimeter was reported to exhibit wide linearity up to 30 Gy before saturation, based on R2-dose response (Watanabe et al., 2022).

The outcomes in Table 1 show the broadening of the linear region with maltose concentration, except for HEMAMAL3, based on changes in absorbance and peak absorbance responses. This reveals maltose's ability to enhance HEMA PGD's linear range. The effect of maltose concentration in elevating peak

absorbance and shifting at doses of 5, 10, 15, 20, 25, and 30 Gy is depicted in Figure 5(A) and (B), respectively.

Combining the curves in Figure 4(A)-(E) with Table 1 reveals a robust correlation between absorbed dose and change in absorbance (ΔA) (R^2 = 0.9840, 0.9997, 0.9792, and 0.9957 for HEMAMAL1, HEMAMAL2, HEMAMAL3, and HEMAMAL4 respectively). Similarly, correlations are evident for peak absorbance (R^2 = 0.9834, 1.0000, 0.9817, and 0.9964), bandwidth (R^2 = 0.9792, 0.9953, 0.9489, and 0.9840), and wave number (R^2 = 0.9643, 0.9920, 0.8253, and 0.9616). The bandwidth (Δλ) signifies the energy range of molecular vibration, as shown in Equation 3, while the wave number ($\tilde{\nu}$) represents molecular vibration frequency, as illustrated in Equations 2–4. These correlations hint at the potential utilization of various energy aspects of molecular vibration (spectral bandwidth), intensity/amplitude (peak absorbance), and frequency (wave number) for translating into absorbed doses.

Effect of Maltose Concentration on Radiation Dose Response

Maltose concentration is observed to impact the response of the studied PGDs, as evident in Figures 4(A)—(E) and Table 1. The impact across varying absorbed dose levels is illustrated in Figures 5(A) and 5(B) based on peak absorbance (Ap) and λ_{max}, respectively.

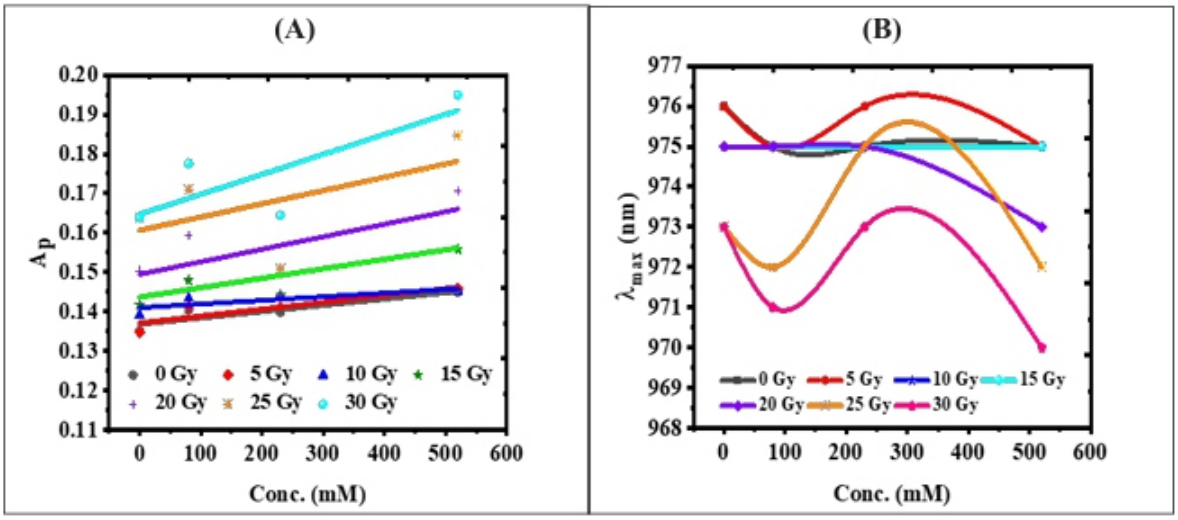

Figure 5. The effect of maltose concentration (A) to increase the peak absorbance and (B) to shift the λ_{max} for absorbed doses of 5, 10, 15, 20, 25, and 30 Gy

An increase in Ap and a decrease in λmax serve as indicators of increased polymerization within the PGD. The overlap between the curves for 10 Gy and 15 Gy and the curve 0 Gy, as observed in Figure 5(B), can, therefore, suggest a deceleration in polymerization when the absorbed dose exceeds 5 Gy until 15 Gy, beyond which there is a resurgence polymerization rate, as evident from the curves for 20 Gy, 25 Gy, and 30 Gy.

Sensitivity

Sensitivity is a key characteristic of PGDs that reflects their ability to respond to radiation. It is determined by the ratio of the change in response to the change in dose, represented by the slope of the linear portion of the fitting curve (Bahrami et al., 2021; Deene, 2004). The sensitivities of four PGDs, namely HEMAMAL1, HEMAMAL2, HEMAMAL3, and HEMAMAL4, sharing the same composition except for maltose concentrations irradiated within the 0-30 Gy range, are illustrated in Figure 6 based on changes in absorbance, bandwidth, peak absorbance, and wave number.

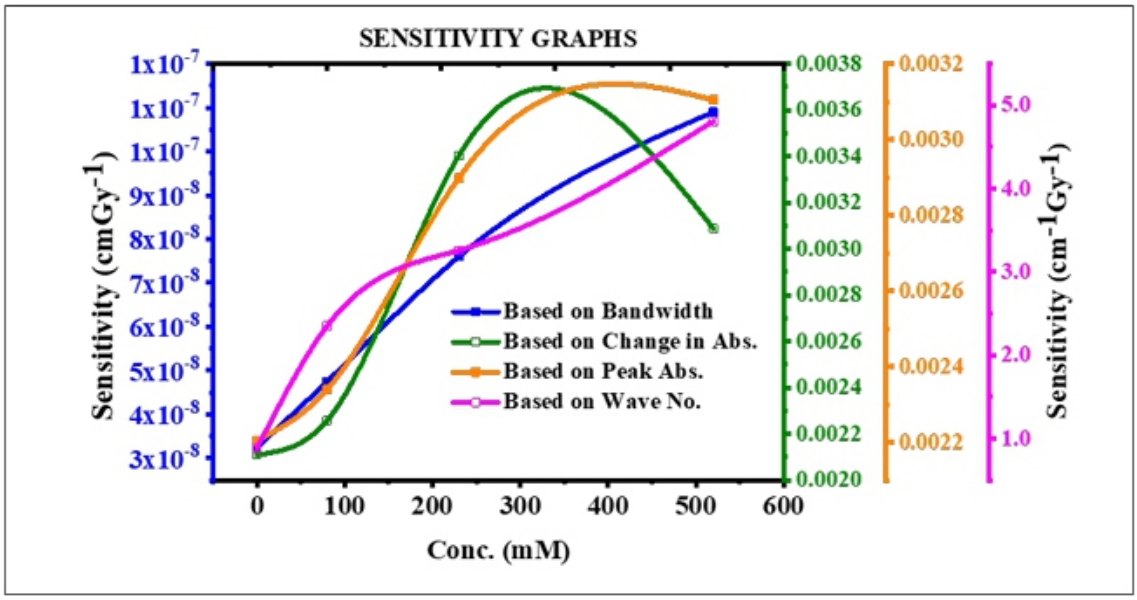

Figure 6. The sensitivity of HEMA PGDs as a function of maltose concentration is based on various measured responses

The findings in Figure 6 reveal an increase in sensitivity with rising maltose concentration. Notably, sensitivities differ across various response types, each carrying its own unit. For bandwidth measured in cm, sensitivity is expressed as $cmGy^{-1}$. In terms of bandwidth, sensitivity increases with maltose concentration up to 520 mM. calculated based on wave number (measured in cm^{-1}) is also expressed in $cm^{-1}Gy^{-1}$. In this context, wave number sensitivity gradually increases within 100-200 mM and a more substantial increase or steeper curve within maltose concentrations of 0-100 mM and 200-520 mM.

Sensitivities based on peak absorbance and change in absorbance are derived from the slope of Beer Lambert's law in equation 1, and they share the unit ($cm^{-1}Gy^{-1}$). These two responses reveal sensitivities reaching peak values of 0.0037 $cm^{-1}Gy^{-1}$ at 329 mM and 0.0032 $cm^{-1}Gy^{-1}$ at 406 mM for change in absorbance and peak absorbance responses, respectively, after which they begin to decline. In parallel, we are concurrently pursuing research to determine the optimal maltose concentration for HEMA PGD, utilizing the UV-Vis readout technique and exploring various options for baseline correction and reference samples.

This outcome underscores the dependence of the sensitivity of PGDs on the composition of their components and the readout technique employed. In a previous study, NIBMAGAT gel dosimeters irradiated within the 0-30 Gy range exhibited a sensitivity of 0.016 $cm^{-1}Gy^{-1}$ based on UV-Vis readout and 0.0775 $s^{-1}Gy^{-1}$ based on NMR (Lotfy et al., 2017). Notably, sensitivity based on UV-Vis can also vary for the same dosimeter, depending on the λmax . As an example, the sensitivity of HEMATAG PGD, composed of HEMA as the monomer, was reported as 0.017, 0.015, 0.013, 0.011, and 0.006 $cm^{-1}Gy^{-1}$ at λmax = 500, 550, 600, 650, and 700 nm respectively (Ishak et al., 2015).

Temporal Stability

A study on the stability of PGD responses after irradiation reveals the continuation of polymerization for several hours. It is attributed to the net flux of fresh monomers from regions of low dose to regions of high dose, where they react with long-living polymer radicals in that region. It can also result from auto-polymerization of monomers or structural changes in the gel matrix. However, this effect is unwanted as it could lead to overestimating the absorbed dose (Aliasgharzadeh et al., 2022; Deene, 2004). The temporal stability of HEMAMAL2 was evaluated and is presented in Figure 7

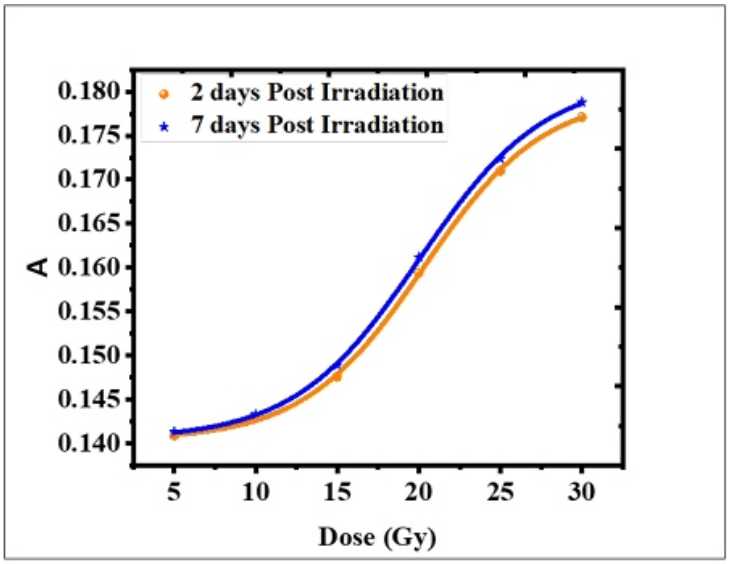

Figure 7. The response of HEMAMAL2 scanned 2 days and 7 days after irradiation

Figure 7 depicts the response curves of HEMAMAL2 scanned 2 days and 7 days post irradiation. These two curves are compared based on the parameters A1 , A2 , logx 0, and p, which describe the sigmoidal dose-response curve given in Equation 6. The comparison results are presented in Table 2.

Table 2
Comparison between the various parameters of HEMAMAL2 scanned 2 days and 7 days post-irradiation

Post Irrad.	A_1	A_2	Log_x0	p ($cm^{-1}Gy^{-1}$)	R^2
2 days	0.1404	0.1796	20.3020 ± 0.17	0.1291 ± 0.01	0.9998
7 days	0.1405	0.1815	20.0347 ± 0.20	0.1134 ± 0.01	0.9995
|Dev.|	0.0001	0.0019	0.2673	0.0057	
%Dev.	0.0712%	1.0579%	1.3166%	4.7859%	

Post Irrad. = Post irradiation time, Dev. = deviation, and %Dev. = Percentage deviation

Table 2 shows that the change in absorbance scanned 7 days post-irradiation deviated from its response 2 days post-irradiation by approximately 0.07% in A1 , 1.1% in A2 , 1.3% in logx 0, and 4.8% in p. The standard errors in A1 and A2 are in the order of 10-4 and are thus considered negligible. This outcome is consistent with temporal stability up to 8 days post-irradiation based on transverse relaxation rate (R2) and optical absorbance readout techniques reported in another study (Lotfy et al., 2017). Similar stability was observed in the PAKAG PGD 7 days post-irradiation (Rashidi et al., 2020).

Temperature Independence

Temperature can significantly impact the response of irradiated PGDs. This effect may stem from a decrease in viscosity as temperature rises (Deene, 2004). The impact of scanning temperature on HEMAMAL2's response was assessed at two distinct temperatures: 22°C and 25°C, as illustrated in Figure 8. The two curves in Figure 8 are comparable based on values like A1 , A2 , logx 0, p, and R2, provided in Table 3.

Table 3
Comparison between the response of HEMAMAL2 scanned at 22°C and at 25°C

Scan. Temp.	A_1	A_2	Log_x0	p ($cm^{-1}Gy^{-1}$)	R^2
22°C	0.1288	0.1678	17.6639 ± 4.6892	0.0872 ± 0.1063	0.9267
25°C	0.1312	0.1670	16.0286 ± 4.8687	0.1099 ± 0.1731	0.8680
|Dev.|	0.0024	0.0008	1.6353	0.0227	
% Dev.	1.8634%	0.4768%	9.2579%	26.0321%	

Scan. Temp. = Scanning Temperature

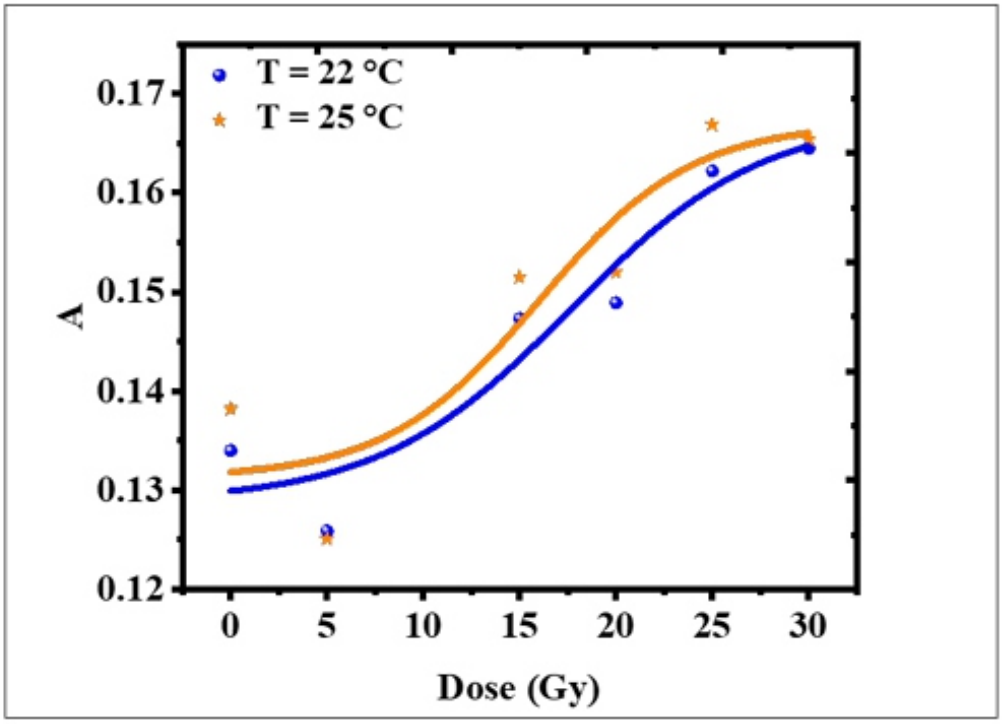

Figure 8. The sigmoidal dose-response curves of HEMAMAL2 scanned at 22°C and 25°C based on absorbance

The examination of Table 3 reveals differences in the lower and upper asymptotes A1 and A2 at 22°C and 25°C, which are approximately 1.9% and 0.5%, respectively. The SE values for A1 and A2 are 10-3 and thus not deemed significant. It suggests relative stability in the span of the dosimeter's response at both temperatures. This finding aligns with the stability observed in the PASSAG gel dosimeter's response, as measured by R2 when scanned within the temperature ranges of 15°C–18°C and 20°C–24°C (Aliasgharzadeh et al., 2022).

However, the sensitivity (p) at 25°C deviates by 0.0227 cm-1Gy-1 (approximately from that at 22°C. This discrepancy can be attributed to the shifting back of the steepest point on the curve to lower dose by 1.6 Gy when scanned at 25°C compared to 22°C, owing to the nature of the Hill's curve. This shift likely arises from structural change or increased mobility of the polymerized and crosslinking molecules at higher temperatures, as this significantly affects the PGD's dose response (Deene, 2004).

Applicability of NIR for PGD Evaluation in Clinical Settings and Future Research

NIR spectroscopy can practically be employed for PGD evaluation in clinical settings by installing a high-quality UV-Vis-IR spectrophotometer with a sample holder suitable for various shapes and sizes of phantoms. Some manufacturers have recently provided two or more sample holders that can be substituted for various shapes and sizes. The device shall be accurately calibrated, evaluated and standardized for consistent dose evaluation Future research on translating molecular vibrational

parameters into 3D images could involve inventing NIR spectral analysis software and algorithms to be integrated into imaging devices or real-time displays that can correlate molecular vibrational changes with the absorbed dose to map 3D dose distribution. Although this could be more complex than ordinary UV-Vis-IR spectroscopy, it might be less time-consuming and more cost-effective.

CONCLUSION

HEMA-based PGDs with maltose additive were fabricated, irradiated within the 0–30 Gy range, and subsequently scanned using a UV-Vis-IR spectrophotometer spanning 7501100 nm. The outcomes demonstrated the feasibility of translating molecular vibrational frequency, amplitude/intensity, and vibration energy into absorbed doses. The linear range and sensitivity expanded as maltose concentration increased. The PGDs' response remained stable for up to 7 days post-irradiation, and this stability was relatively unaffected by scanning temperature. In conclusion, IR spectroscopy presents a potentially more costeffective means of reading HEMA PGDs. Furthermore, the addition of maltose within the range of 0–520 mM exhibited the capacity to enhance both sensitivity and linear dose responses of the PGDs. These findings promise to enhance the affordability of radiotherapy procedures for underserved populations while bolstering the efficiency of PGD dosimetry in clinical radiotherapy. We finally recommend further research into translating the molecular vibrational parameters into 3D images.

ACKNOWLEDGEMENT

We appreciate the account of the Postgraduate Grant, School of Physics, USM (No Akaun: 308.AIFIZIK.415403) for financial support to purchase reagents. We also extend our gratitude to the technical assistance provided by the Department of Biomedical Imaging, Advanced Medical and Dental Institute, USM, Mr. Mohd Rizal Mohammad Rodin, and Mr. Hazhar Hassan, both from the School of Physics, USM

REFERENCES

Abdel-Ghany, A. M., Abu-Khadra, A. S., & Sadeq, M. S. (2020). Influence of Fe cations on the structural and optical properties of alkali-alkaline borate glasses. Journal of Non-Crystalline Solids, 548, Article 120320. https://doi.org/10.1016/j.jnoncrysol.2020.120320

Adliene, D., Urbonavicius, B. G., Laurikaitiene, J., & Puiso, J. (2020). New application of polymer gels in medical radiation dosimetry: Plasmonic sensors. Radiation Physics and Chemistry, 168, Article

108609. https://doi.org/10.1016/j.radphyschem.2019.108609

Al-Jarrah, A. M., Rahman, A. A., Shahrim, I., Razak, N. N. A. N. A., Ababneh, B., & Tousi, E. T. (2016). Effect of inorganic salts and glucose additives on dose–response, melting point and mass density of genipin gel dosimeters. Physica Medica, 32(1), 36–41. https://doi.org/10.1016/j.ejmp.2015.09.003.

Aliasgharzadeh, A., Anaraki, V., Khoramian, D., Ghorbani, M., & Farhood, B. (2022). The impact of various amounts of fabricating components on the response of PASSAG polymer gel dosimeter: An optimization study. Radiation Physics and Chemistry, 190, Article 109804. https://doi.org/10.1016/j.radphyschem.2021.109804

Bahrami, F., Abtahi, S. M. M., Sardari, D., & Bakhshandeh, M. (2021). Investigation of a modified radiochromic genipin-gel dosimeter: Dosimetric characteristics and radiological properties. Journal of Radioanalytical and Nuclear Chemistry, 328(1), 19–31. https://doi.org/10.1007/s10967-021-07635-w

Darwish, S. M., & Darwish, I. M. (2022). Spectroscopic investigation of tau protein conformational changes by static magnetic field exposure. Journal of Physics Communications, 6(7), Article 075004. https://doi. org/10.1088/2399-6528/ac7d3a

Deene, Y. D. (2022). Radiation dosimetry by use of radiosensitive hydrogels and polymers: Mechanisms, stateof-the-art and perspective from 3D to 4D. Gels, 8(9), Article 599. https://doi.org/10.3390/gels8090599

Deene, Y. D. (2004). Essential characteristics of polymer gel dosimeters. Journal of Physics: Conference Series, 3, 34–57. https://doi.org/10.1088/1742-6596/3/1/006.

Farajollahi, A. R., Bonnett, D. E., Ratcliffe, A. J., Aukett, R. J., & Mills, J. A. (1999). An investigation into the use of polymer gel dosimetry in low dose rate brachytherapy. The British Journal of Radiology, 72(863), 1085–1092. https://doi.org/10.1259/bjr.72.863.10700826

Gadagkar, S. R., & Call, G. B. (2015). Computational tools for fitting the hill equation to dose-response curves. Journal of Pharmacological and Toxicological Methods, 71, 68–76. https://doi.org/10.1016/j.vascn.2014.08.006

Ishak, S. A., Iskandar, S. M., & Rahman, A. A. (2015). Sensitivity of HEMATEG induced by radiation dose in the diagnostic X-Ray energy range. Advanced Materials Research, 1087, 267–271. https://doi.org/10.4028/ www.scientific.net/AMR.1087.267

Jaszczak, M., Maras, P., & Kozicki, M. (2020). Characterization of a new N -vinylpyrrolidone-containing polymer gel dosimeter with Pluronic F-127 gel matrix. Radiation Physics and Chemistry, 177, Article 109125. https://doi.org/10.1016/j.radphyschem.2020.109125.

Javaheri, N., Yarahmadi, M., Refaei, A., & Aghamohammadi, A. (2020). Improvement of sensitivity of X-ray CT reading method for polymer gel in radiation therapy. Reports of Practical Oncology & Radiotherapy, 25(1), 100–103. https://doi.org/10.1016/j.rpor.2019.12.017

Kipouros, P., Pappas, E., Baras, P., Hatzipanayoti, D., Karaiskos, P., Sakelliou, L., Sandilos, P., & Seimenis, I. (2001). Wide dynamic dose range of VIPAR polymer gel dosimetry. Physics in Medicine and Biology, 46(8), 2143–2159. https://doi.org/10.1088/0031-9155/46/8/308

Kozicki, M., Berg, A., Maras, P., Jaszczak, M., & Dudek, M. (2020). Clinical radiotherapy application of N-vinylpyrrolidone-containing 3D polymer gel dosimeters with remote external MR-reading. Physica Medica, 69, 134–146. https://doi.org/10.1016/j.ejmp.2019.11.014

Lotfy, S., Basfar, A. A., Moftah, B., & Al-Moussa, A. A. (2017). Comparative study of nuclear magnetic resonance and UV–visible spectroscopy dose-response of polymer gel based on N-(Isobutoxymethyl) acrylamide. Nuclear Instruments and Methods in Physics Research, Section B: Beam Interactions with Materials and Atoms, 413, 42–50. https://doi.org/10.1016/j.nimb.2017.09.033.

Masithoh, R. E., Pahlawan, M. F. R., Saputri, D. A. S., & Abadi, F. R. (2023). Visible-near-infrared spectroscopy and chemometrics for authentication detection of organic soybean flour. Pertanika Journal of Science and Technology, 31(2), 671–688. https://doi.org/10.47836/pjst.31.2.03

Mustaqim, A. S., Yahaya, N. Z., Razak, N. N. A., & Zin, H. (2020). The dose enhancement of MAGAT gel dosimeter doped with zinc oxide at 6 MV photon beam. Radiation Physics and Chemistry, 172, Article108739. https://doi.org/10.1016/j.radphyschem.2020.108739

Nezhad, Z. A., & Geraily, G. (2022). A review study on application of gel dosimeters in low energy radiation dosimetry. Applied Radiation and Isotopes, 179, Article 110015. https://doi.org/10.1016/j.apradiso.2021.110015

Nezhad, Z. A., Geraily, G., Parwaie, W., & Zohari, S. (2021). A novel investigation of the effect of different concentrations of methacrylic acid on the dose response of MAGAT gel dosimeter in intraoperative radiotherapy. Radiation Physics and Chemistry, 179, Article 109214. https://doi.org/10.1016/j.

radphyschem.2020.109214

Ozaki, Y. (2021). Infrared spectroscopy—mid-infrared, near-infrared, and far-infrared/terahertz spectroscopy. Analytical Sciences, 37(9), 1193–1212. https://doi.org/10.2116/analsci.20R008.

Pratiwi, R. A., Bayu, A., & Nandiyanto, D. (2022). How to read and interpret UV-VIS spectrophotometric results in determining the structure of chemical compounds. Indonesian Journal of Educational Research and Technology, 2(1), 1–20. https://doi.org/10.17509/xxxx.vxix

Rabaeh, K. A., Hammoudeh, I. M. E., Oglat, A. A., Eyadeh, M. M., Abdel-Qader, A. J., Aldweri, F. M., & Awad, S. I. (2021). Polymer gel containing N,N'-methylene-bis-acrylamide (BIS) as a single monomer for radiotherapy dosimetry. Radiation Physics and Chemistry, 187, Article 109522. https://doi.org/10.1016/j. radphyschem.2021.109522

Rashidi, A., Abtahi, S. M. M., Saeedzadeh, E., & Akbari, M. E. (2020). A new formulation of polymer gel dosimeter with reduced toxicity: Dosimetric characteristics and radiological properties. Zeitschrift Für

Medizinische Physik, 30(3), 185–193. https://doi.org/10.1016/j.zemedi.2020.02.002

Renner, I. E., & Fritz, V. A. (2020). Using near-infrared reflectance spectroscopy (NIRS) to predict glucobrassicin concentrations in cabbage and brussels sprout leaf tissue. Plant Methods, 16(1), Article 136. https://doi.org/10.1186/s13007-020-00681-7

Shih, T. Y., Chen, W. T., Kuo, W. C., & Wu, J. (2022). Application of polarization-sensitive optical coherence tomography in measurement of gel dosimeters. Journal of Medical and Biological Engineering, 42(5), 621–629. https://doi.org/10.1007/s40846-022-00711-w

Shukor, N. S. A., Musarudin, M., Abdullah, R., & Aziz, M. Z. A/ (2022). Dose distribution of 192Ir HDR brachytherapy source measurement using gafchromic® EBT3 film dosimeter and TLD-100H. Pertanika Journal of Science and Technology, 30(1), 691–708. https://doi.org/10.47836/pjst.30.1.37

Watanabe, Y., Maeyama, T., Mizukami, S., Tachibana, H., Terazaki, T., Takei, H., Muraishi, H., Gomi, T., & Hayashi, S. I. (2022). Verification of dose distribution in high dose-rate brachytherapy for cervical cancer using a normoxic N-vinylpyrrolidone polymer gel dosimeter. Journal of Radiation Research, 63(6), 838–848. https://doi.org/10.1093/jrr/rrac053.

Zapata, F., López-Fernández, A., Ortega-Ojeda, F., Quintanilla, G., García-Ruiz, C., & Montalvo, G. (2021). Introducing ATR-FTIR spectroscopy through analysis of acetaminophen drugs: Practical lessons for interdisciplinary and progressive learning for undergraduate students. Journal of Chemical Education, 98(8), 2675–2686. https://doi.org/10.1021/acs.jchemed.0c01231

ISSN 0128-7680

The Impact of Hydrocarbon R290 Refrigerant on Air Conditioner Performance and Environmental Sustainability

Ferdinand Ng Siek Khai1,2 and Nurul Sabihah Zakaria1*

1School of Distance Education, Universiti Sains Malaysia (USM), 11800 Minden, Pulau Pinang, Malaysia
2Ener-Save Green Air Conditioner Sdn Bhd, 29A, Jalan Ronggeng 11, Taman kudai, Johor Bahru, 81300 Johor, Malaysia

ABSTRACT

This study addresses the critical need for environmentally friendly refrigerants in residential air conditioning systems and explores the advantages of hydrocarbon R290 as an alternative to synthetic options. Given the indispensability of air conditioning for human comfort, the shift towards ecofriendly refrigerants becomes paramount. This research aims to demonstrate the superiority of natural refrigerants, particularly hydrocarbon R290, over conventional synthetic alternatives in air conditioning. Through a comparison of two similar air conditioners charged with R290 and R22 refrigerants, the study evaluates their performance and environmental implications. The initial phase involves a thorough analysis of hydrocarbon R290's physical properties and compatibility with synthetic refrigerants. The findings underscore its remarkable compatibility, directly replacing the environmentally harmful Hydrochlorofluorocarbon R22 refrigerant. Practical experiments and theoretical pressure-enthalpy chart analyses establish that R290-equipped air conditioners significantly enhance the coefficient of performance (COP). In practical applications, COP sees a 21.74% boost, while theoretical analysis indicates a 7.33% increase. Furthermore, adopting R290 contributes to a 17.5% reduction in CO2 emissions through reduced power consumption. Environmental sustainability is a pivotal aspect of refrigerant evaluation; the study furnishes compelling evidence favouring hydrocarbon R290. The research demonstrates that R290 is approximately 1,383 times more environmentally friendly than R22 in terms of global warming potential and refrigerant mass. Safety, a paramount concern in adopting new refrigerants, is also addressed. R290's mass charge aligns with international standards, and its concentration remains 17.37% below the lower flammability limit, ensuring secure usage in confined spaces.

Keywords: *Hydrocarbon R290, air conditioner, coefficient of performance, global warming potential, environmental sustainability, natural refrigerant*

INTRODUCTION

Global issues such as the energy crisis, the ozone-depleting threat, the impact of global warming and climate change require more public attention. How are these pressing issues interrelated to the heating, ventilation and air conditioning (HVAC) industry?

In the earlier stage of phasing out ozone-depleting substances, most appliances were replaced by non-

ozone-depleting refrigerants, mainly formulated by fluorinated gases (F-gases), specifically hydrofluorocarbon (HFC), as an alternative to ozone-depleting refrigerants. However, Europe considers these F-gases powerful greenhouse gases (European Commission, 2022). As a result, some European countries have opted to switch from HFCs to other superior refrigerants or natural refrigerants.

The Kigali Amendment to the United Nations (UN) Montreal Protocol is another effort to reduce global temperature after the success of the UN Montreal Protocol program. It aims to continue addressing the climate change problem by eliminating powerful greenhouse gases and, if faithfully implemented, could control the full rise of 0.5 degrees Celsius in global temperature by the end of the century (United Nations Climate Change, 2016) (2100). Malaysia ratified the Kigali Amendment to the UN Montreal Protocol on 21 October 2020 (Ministry of Environment and Water, 2020). As a result, Malaysia is obligated to phase down the high global warming HFCs based on the Malaysian Baseline. The first phase down of 10% is scheduled for 2029, with a further 20% of the balance from the baseline allowed for essential uses by 2045.

The hydrocarbon R290 refrigerant is highly flammable, but it is suitable for use as a conversion option for existing R22 refrigerant air conditioners without requiring major retrofitting of the existing system. The primary and only challenge with refrigerants is their high flammability. However, this concern can be addressed through refrigerant mass charge control, and the HVAC design must comply with international A3class refrigerant safety standards. Even though the hydrocarbon refrigerant air conditioners require such a safety design, the manufacturing cost is not significantly affected because the compressor is built with explosion-proof mild steel, the copper tubes are sparkless, and the system operates under an oxygen-free circuit. Moreover, the cost of natural refrigerants is much lower than that of synthetic refrigerants. The molecular mass of hydrocarbon R290 refrigerant is lighter than that of existing R22 refrigerant. However, it has a similar volumetric charge, which can further reduce the compressor power consumption and enhance lifespan.

Synthetic refrigerants are widely used in the market but significantly impact warming. They are super greenhouse gases. These synthetic refrigerants also contribute to the pollution of freshwater sources through trifluoroacetate (TFA) in the atmosphere (Rusyanto, 2021). As scientists have reported, TFA is a chemical compound generated the latest invented synthetic refrigerants known as hydrofluoric-olefins (HFOs).

Figure 1 shows global greenhouse gas emissions by variable types of gases. The source is the Intergovernmental Panel on Climate Change (IPCC) (2014), based on global emissions from 2010

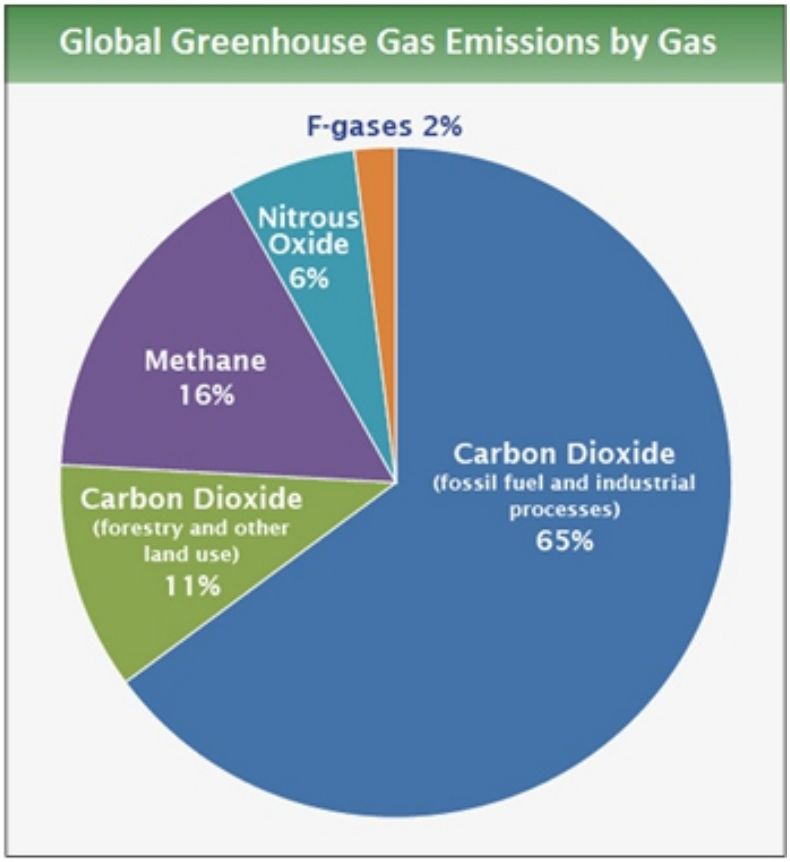

Figure 1. Global greenhouse gas emissions

The air conditioner industry is phasing out the ozone-depleting refrigerants and replacing them with newer alternatives. However, most of the refrigerants used today are high global warming substances. Surprisingly, just two per cent of F-gas refrigerants are the main contributors to Global Warming Source. The impact of this 2% from the F-gases can be significant. On the other hand, if natural refrigerants replace these refrigerants, the reduction in global warming could be substantial and beneficial for mankind. According to the Sustainable Energy Development Authority (SEDA) Malaysia's 2016 Co2 emissions report, Peninsular Malaysia's Co2 emission coefficient rate is 0.639 kg per kWh of electrical usage (SEDA Malaysia, 2019).

As air conditioning systems have become essential for human comfort, the transition to eco-friendly refrigerants is becoming increasingly important. This research aims to demonstrate the superiority of natural refrigerants, specifically hydrocarbon R290, over traditional synthetic refrigerants in air conditioning applications.

MATERIALS AND METHODS

Preliminary prototype setups are required for a system with R290 refrigerant, and the other unit is

charged with R22 Refrigerant for data findings and studying. Instruments to measure the temperature, pressure, airflow and electrical parameters are installed on the prototypes. The important part of prototype setup is ensuring the systems are free from leakage problems. Any faults should be rectified before being charged with refrigerant. Prototypes are vacuumed thoroughly and charged with R290 and R22 refrigerant, respectively. Once the systems have been completely functionally tested, the results will be observed and f ine-tuned to meet the required discharge pressure, suction pressure, temperature, air flow rate and power consumption. Neither system should be undercharged nor overcharged with refrigerant. The data findings will further plot the pressure-enthalpy chart and compute the obtained cooling capacity. Subsequently, other related results will be derived via recorded raw data such as refrigerant mass flow, work done during compression, electrical power, Co2 equivalent emissions and coefficient of performance.

The thermodynamic properties and compatibility study were obtained from the "EnerSave Hydrocarbon Refrigerants Training Manual" (Ng, 2021). This information is essential to identify whether the existing domestic air conditioner is suitable for conversion into a Hydrocarbon natural refrigerant system or whether any modification is required to retrofit it.

Table 1 contains the basic information related to refrigerants' physical and properties and related information on R290 refrigerant and R22 refrigerant. R290 refrigerant is an organic natural refrigerant; it is propane hydrocarbon with a chemical compound of C3 H8 , and the R22 refrigerant is a synthetic refrigerant with a chemical compound of hydrochlorofluorocarbon (CHClF2). The R290 refrigerant is an environmentally friendly refrigerant with zero ozone-depleting potential and negligible global warming potential compared to the R22 refrigerant. The atmospheric life of R290 refrigerant is much shorter than that of R22 refrigerant, making it less harmful to the environment.

While the boiling point of R290 refrigerant is approximately the same as that of R22 refrigerant, due to its lower molecular weight, R290 refrigerant appears to be lighter than R22 refrigerant. The R290 refrigerant also has a higher heat absorption value than the R22 refrigerant, attributed to its latent heat of vaporization value at its boiling point. Mineral oil is the compressor lubricant oil compatible with R290 and R22 refrigerants. This compatibility enables the conversion of existing R22 refrigerant domestic air conditioners to R290 refrigerant, in addition to the general compatibility with other elastomeric materials.

According to the safety classification from ASHRAE Standard 34, refrigerants are categorized into different safety classes based on their chemical characteristics (ASHRAE, 2022). R290 refrigerant is

classified as A3 due to its lower toxicity and high flammability. On the other hand, the R22 refrigerant is classified as an A1 refrigerant with lower toxicity and non-flammability.

Table 1
Physical properties, chemical properties, and related information of R290 refrigerant and R22 refrigerant

Descriptions	**Column of Comparison**	
Refrigerant Type	R290	R22
Chemical Type	HC (Hydrocarbon)	HCFC (Hydrochloro- fluorocarbon)
Global Warming Potential (GWP), CO_2 = 1, 100 years basis	3	1,810
Ozone Depleting Potential (ODP)	0	0.055
Atmospheric Life	< 1 year	12 years
Boiling Point (°C)	-42	-41
Molecular Weight,	44.1 g/mol	86.5 g/mol
Latent Heat of Vaporisation @ Boiling Point kJ/kg	426	233
Compressor Lubricant Oils	Mineral or Synthetic Oil	Mineral Oil Only
ASHRAE Standard 34 Refrigerant Safety Classification	A3 Lower toxicity, highly flammable	A1 Lower toxicity, Non-flammable
Leak Detection Method	Hydrocarbon	Halide
Autoignition (°C)	480	NA
Lower Flammability Limit (LFL), kg/m^3	0.038	NA
Toxic Thermal Decomposition	None	Phosgene Gas

The air conditioning system consists of four major components that correspond to the Carnot refrigeration cycle (Cengel & Boles, 2015). These components include the expansion valve for the adiabatic expansion process, the evaporator coil for the isothermal expansion process, the compressor for the adiabatic compression process, and the outdoor condenser coil for the isothermal compression process. This closed-loop cycle uses refrigerant as a heat transfer medium, absorbing heat from the indoor area of the house and releasing it to the outdoor environment. It represents the typical usage of an air conditioner in hot climate countries.

Practically all the different types of refrigerants have different enthalpy properties. Equation 1 gives the relationship of enthalpy, h.

$$h = E_{int} + pv \quad [1]$$

Where E_{int} is the total internal energy

Pressure-enthalpy charts will be plotted based on the actual performance of the prototype setup to simplify the determination of the work done for air conditioners using different refrigerants. This setup includes an R290 refrigerant air conditioner with pressure gauges, temperature displays, and a similar setup charged with R22 refrigerant. Figure 3 describes the plotting of the pressure-enthalpy chart; the temperatures and pressures are obtainable parameters from the prototype setup. The compressor drives the whole system as a main driver. Thus, the intention to determine the air conditioner's coefficient of performance will focus on the compression process as it will consume external energy to perform work internally. Even though the condenser fan motor and evaporative fan motor are used to transfer internal heat from the system out to the outdoor environment and from the external heat source of the indoor house to the internal refrigeration system, respectively, the energy of such fan motor is lesser than the energy consumed by the compressor. Therefore, the main focus of the study on the theoretical performance will be narrowed to the compression process, and the formula to obtain the work done during the compression of refrigerant is as Equation 2.

$$Q_c = m_R \times (h_2 - h_1) \quad [2]$$

Where m_R is the mass flow of refrigerant

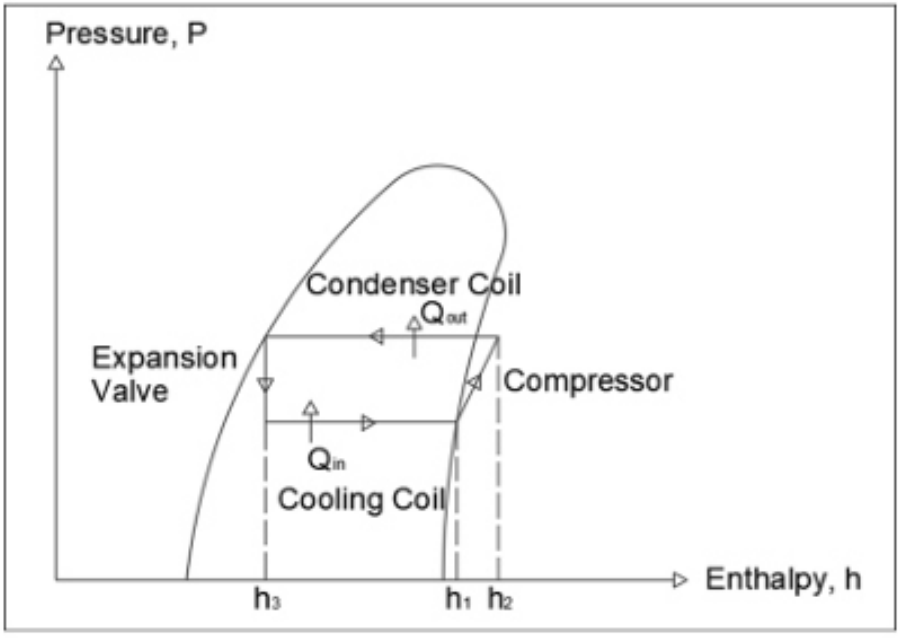

Figure 2. Pressure: Enthalpy diagram of the refrigeration system and the components involved

Ultimately, the coefficient of refrigerant performance in the system between natural R290 refrigerant and synthetic R22 refrigerant will be compared and calculated.

Firstly, the refrigerating effect per kg, RE , can be obtained from Equation 3 before calculating the mass flow of refrigerant.

$$R_E = h_1 - h_3 \quad [3]$$

After finding the RE value, Equation 4 shows the refrigerant's mass flow, mR . The cooling capacity is the actual cooling performance of the air conditioner's evaporative
blower.

m_R = cooling capacity / R_E
Thus,

$$m_R = \text{cooling capacity} / (h_1 - h_3) \quad [4]$$

and

The work done during refrigerant compression, Qc (Equation 5), is the interesting part of identifying the work done on the air conditioner's compressor, as it is the main driver of the closed-loop thermodynamic process.

$$Q_c = m_R \times (h_2 - h_1) \quad [5]$$

Nevertheless, the theoretical coefficient of performance (COP) for the refrigerant can be obtained from Equation 6

$$COP = (h_1 - h_3) / (h_2 - h_1) \quad [6]$$

Classically, the cooling capacity was calculated using the imperial unit in most applications; certain conversions are required to identify whether the calculated value matches within the range of design or not. Such as:

1 Watt = 3.412 btu/hour (Cooling Capacity) = 1 Joule/s
1 horsepower (hp) = 741 Watt (Electrical Power)
12,000 btu/hour = 1 refrigeration ton (RT)

Practically, the higher the specific power value, the lower the air conditioner's coefficient of performance. Higher specific power means the air conditioning system consumes more energy to produce a refrigeration ton of cooling. The specific power could be obtained from Equation 7.

$$\text{Specific Power} = \frac{\textit{Electrical Power}}{\textit{Refrigeration Ton}} \quad [7]$$

COP is always inversely proportional to a specific power, as shown in Equation 8.

$$\text{COP} = 12 / (\text{Specific Power} \times 3.412) \quad [8]$$

Specific heat at constant pressure (C_p) is required to raise the temperature of a unit mass of gas by one degree Celsius at constant atmospheric pressure (Khurmi & Gupta, 2008).

Total heat energy, Q, is equal to the mass of air multiplied by its specific heat at constant pressure with the differential temperature obtained, as shown in Equation 9.

$$Q = m\, C_p\, (T_{in} - T_{out}) \quad [9]$$

Where T_{in} enters air temperature (data collection from prototype), and T_{out} leaves air temperature (data collection from prototype). Hence, if the thermodynamic takes place, the derivation of heat energy Q is the cooling capacity from the evaporator and is derived in Equation 10.

$$\text{Cooling capacity, } dQ/dt = (m/dt)\, C_p\, (T_{in} - T_{out}) \quad [10]$$

Where the m/dt is the mass flow rate of air or M_f.

The mass of air is given by Equation 11.

$$\text{Mass of air, } m = \text{density of air} \times \text{volume of air} \quad [11]$$

However, the airflow from the evaporative blower is a dynamic property. The airflow rate from the evaporative blower must be measured to get the mass flow rate of air. Equation 12 is the formula to find the mass flow rate of air.

$$M_f = \text{density of air } (kg/m^3) \times \text{air flow rate } (m^3/s) \quad [12]$$

Therefore, the air conditioner's final and simplified cooling capacity can be estimated using Equation 13.

$$\text{Cooling capacity} = M_f \times C_p (T_{in} - T_{out}) \quad [13]$$

Figures 3 and 4 show a complete prototype setup with a temperature sensor, pressure gauge, power logger and air flow meter. One of the air conditioners is charged with 240 grams of R290 refrigerant, and the other is charged with 550 grams of R22 refrigerant for virtual comparison and data finding. Both systems switch on for approximately thirty minutes to achieve stabilisation before performing data collection.

Figure 3. Complete indoor evaporator blower setup with measurement gadget

Figure 4. Complete outdoor compression condenser unit setup with measurement gadget

Never forget to conduct the Hydrocarbon conversion according to the standard operating procedure (SOP) because the R290 refrigerant is hydrocarbon and highly f lammable. Table 2 is the practical SOP for conducting the R290 refrigerant conversion in the R22 domestic air conditioner

Table 2
Standard of procedure for R290 conversion

Working procedures	Instructions
Step 1	Perform a leak test after setting up the air conditioner system
Step 2	Estimate equivalent HC charge—Use conversion rate of R22 to R290
Step 3	Check the maximum practical charge limit and consult the MS2678:2017
Step 4	Ensure all tools and working areas are safe from fire hazards and prepare a fire extinguisher.
Step 5	Identify all potential sources of ignition that are out of range
Step 6	Vacuum the air conditioner system thoroughly
Step 7	Using the refrigerant mass charge method to charge in the estimated R290 refrigerant
Step 8	Put a temporary flammable zone at the drop-in working area
Step 9	Apply relevant system marking with a warning sign
Step 10	Switch on the air conditioner and fine-tune the system

The steps to identify the maximum allowable hydrocarbon refrigerant charge in a specific room are outlined in the standard, defined by the installation location. It is recommended that the Malaysian Standard MS 2678:2017 (MS2678 Working Group, 2017) be consulted, where the relevant charge size shall not be more than 20% LFL of hydrocarbon refrigerant charge. If the facility is below ground level, the maximum charge would be 1kg in all circumstances, but not more than 20% LFL of hydrocarbon refrigerants charge.

Equation 14 calculates the maximum hydrocarbon charge size per sealed system in a specific machinery room. Therefore, the gas leak will not trigger the ignition level five times lower than the LFL level. In all circumstances, the leakage event will not occur catastrophically in more than one compressor.

$$m_r = 0.20 \times (LFL) \times v_{room} \quad [14]$$

Where,
LFL = lower flammability limit of refrigerant (kg/m^3) from Table 1,
v_{room} = room volume (m^3)
m_r = refrigerant mass (kg)

RESULTS AND DISCUSSIONS

The study uses the "ELIWELL" IDPlus974 Thermostat for temperature display. It is a dual sensor system consisting of temperature probes 1 (Pb1) and 2 (Pb2), as shown in Figure 5. The study uses the common air ambient temperature (Figure 6) and water medium temperature (Figure 7) to cross-check the sensible detection reading on temperature probes and both temperature displays and to determine the accuracy of both temperature detections. The temperature reading was observed and recorded in Table 3.

Figure 5. "ELIWELL" IDPlus974 Thermostat Schematic Diagram and Wiring Termination

Table 3
Temperature reading of the Pb1 and Pb2 in ambient air temperature and water medium temperature

Medium of Calibration	Probe 1, Pb1		Probe 2, Pb2	
	AC01 (R290)	AC02 (R22)	AC01 (R290)	AC02 (R22)
In Ambient Air (30/03/23, 10.05am)	30.2 °C	30.2 °C	30.1 °C	29.8 °C
In Water Medium (Trial 1, 30/03/23, 10.13 am)	29.4 °C	29.4 °C	29.3 °C	28.8 °C
In Water Medium (Trial 2, 30/03/23, 10.40 am)	29.4 °C	29.4 °C	29.3 °C	28.8 °C

Figure 6. Temperature sensor calibration check in ambient air

Figure 7. Temperature sensor calibration check in water medium

The temperature reading from the Probe 1 sensor is similar, either displayed from AC01 or AC02; thus, Pb1 is used as the main temperature sensor to observe the leaving air temperature. However, the Pb2 from AC01 is less than 0.1oC. Therefore, a +0.1oC calibration adjustment is required from the thermostat, but the AC02's Pb2 is required to adjust +0.4oC to match the actual reading from the thermostat installed at AC02. The calibrations of the temperature reading will be hereafter.

Both air conditioners operated for approximately thirty minutes to keep the refrigeration cycle steady. The raw data are recorded in Table 4. The R290 refrigerants are natural organic compounds, and the R22 refrigerant is synthetic.

Table 4
Air conditioners' operating parameter

Descriptions	**R290 Refrigerant Air Conditioner AC01**	**R22 Refrigerant Air Conditioner AC02**
Refrigerant Mass Charge in 9,000 btu/hr air conditioner	240 grams	550 grams
Suction Pressure in 9,000 btu/hr air conditioner	6.0 Bar/ 0.60 MPa	6.0Bar/ 0.60 MPa
Discharge Pressure in 9,000 btu/hr air conditioner	16 Bar/ 1.6 MPa	18 Bar/ 1.8 MPa
A/C Temperature Set Point (°C)	25	25
Entering Air Temperature °C, T_{in} (Calibrated)	31.5 + 0.1 =**31.6**	31.2 +0.4 = **31.6**
Leaving Air Temperature °C, T_{out}	22.8	22.6
Evaporator Blower, airflow speed, m/s	4.3	4.2
Instant Voltage Reading, V	235.9	236.3
Instant Current Reading, A	3.21	3.92
Power Supply Frequency, Hz	50.1	50.0
Instant Real Power, kW	0.735	0.893
Instant Power Factor, PF	0.970	0.965
Instant Reactive Power, kVar	0.186	0.244

Referring to Table 4, the refrigerant mass charge for the R290 refrigerant air conditioner is 240 grams, while for the R22 refrigerant air conditioner, it is 550 grams. It demonstrates that the refrigerant used in the R290 air conditioner is 56.36% lighter than the R22 refrigerant. The R290 system operates at a low head pressure of approximately 1.6 MPa, despite having a similar suction pressure of 0.6 MPa for both systems. The combination of low head pressure and lighter molecular weight contributes to a reduction in compressor torque power. These characteristics further explain the ability of R290 to enhance energy savings, as the compressor requires less energy to operate the air conditioning system.

The conversion to R290 and the use of R290 refrigerant in R22 domestic air conditioners comply with safety standards. A typical 9,000 BTU/hr air conditioner is installed in a 36-cubic-meter room (3m × 4m × 3mH). The concentration of R290 refrigerant from a 9,000 BTU/hr air conditioner in the room is determined by dividing the refrigerant mass charge per sealed system by the room volume. In the case of a 9,000 BTU/hr R290 air conditioner in a room of 36 cubic meters, the concentration is 0.0066 kg/m^3 in the event of refrigerant leakage. This concentration adheres to the standard that does not exceed 500g and is less than 20% of the lower flammability limit (LFL) charge limit. In fact, it is 17.37% lower than the LFL charge limit.

Cooling Capacity of R290 Air Conditioner and R22 Air Conditioner

The air conditioners were set to a temperature set point of 25°C. The set point does not affect the constant airflow temperature of the indoor evaporator since the testing site is open to the outdoor ambient air. The outdoor ambient temperature thoroughly influences the indoor temperature, thus consistently maintaining the entering air temperature above the set point. As a result, the compressor operates at a 100% load.

From the Equation 13, cooling capacity = $M_f \times C_p (T_{in} - T_{out})$
Specific heat of air at constant pressure, C_p = 1.000kJ/kg.°C
Density of air at 25°C, ρ = 1.1839 kg/m^3

Mf can be obtained from Equation 15; the cooling capacity is calculated separately for the R290 and R22 systems. The airflow rate of the evaporator blower is Vf.

$$V_f(m^3/s) = L \times H \times \text{air-flow speed (m/s)} \quad [15]$$

L = length of evaporator blower = 0.675m
H = height of evaporator blower = 0.080m
The airflow speed is recorded in Table 4

Cooling Capacity of R290 System

The system converted to R290 refrigerant is not working 100% to the designed cooling capacity. Calculating the actual cooling capacity is required to identify the air conditioner's performance. Thus, the parameters required to calculate the cooling capacity are taken from the data collections.

The R290 refrigerant air conditioner is currently operating at 8,254.0 BTU/hr, which is 8.29%, slightly below the designed specification of 9,000 BTU/hr. The cooling capacity falls within an acceptable range, meeting the criteria of being within plus or minus 10% of the 9,000 BTU/hr design.

Cooling Capacity R22 System

The R22 refrigerant system is not working 100% to the designed cooling capacity. Calculating the cooling capacity is required to notify the conditioner's performance air. Thus, the parameters required to calculate the cooling capacity are taken from the data collections.

The R22 refrigerant air conditioner is currently operating at 8,245.4 BTU/hr, which is 8.38%, slightly below the designed specification of 9,000 BTU/hr. The cooling falls within an acceptable range, meeting the criteria of being within plus or minus 10% of the 9,000 BTU/hr design.

Refrigeration Cycle State Analysis

Figure 8 illustrates the operation flow of a refrigeration cycle involving pressure measures. It will then plot the ideal refrigeration cycle in a pressure-enthalpy (p-h) chart. Table 5 summarizes the data found in the p-h chart for every state.

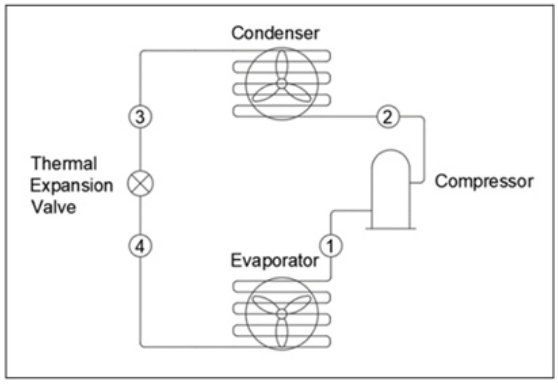

Figure 8. The simple refrigeration cycle diagram involves processes in states 1, 2, 3 and 4. It is a closed-loop cycle from state 1 to state 4 and back to state 1

Table 5
Ideal refrigeration cycle state and data finding summary

Descriptions	State 1	State 2	State 3	State 4
R290 Refrigerant Cycle	p_1 = 6.0 Bar/ 0.60MPa T_1 = 13.46°C h_1 = 479kJ/kg	p_2 = 16 Bar/ 1.60Mpa T_2 = 49.68 °C h_2 = 529kJ/kg	$p_3 = p_2$ $T_3 = (T_2 -$ Subcooling) $h_3 = h_4 = 228$kJ/kg	$p_4 = p_1$ $T_4 = (T_1 -$ Superheat) $h_4 = h_3 = 228$kJ/kg
R22 Refrigerant Cycle	p_1 = 6.0 Bar/ 0.60Mpa T_1 = 10.98°C h_1 = 407kJ/kg	p_2 = 18Bar/ 1.80Mpa T_2 = 49.06 °C h_2 = 438kJ/kg	$p_3 = p_2$ $T_3 = (T_2 -$ Subcooling) $h_3 = h_4 = 262$kJ/kg	$p_4 = p_1$ $T_4 = (T_1 -$ Superheat) $h_4 = h_3 = 262$kJ/kg

Mass Flow of Refrigerant, Work Done and COP

From the pressure-enthalpy chart plotted in Figures 9 and 10, the refrigerating effect per kg could be obtained from Equation 3

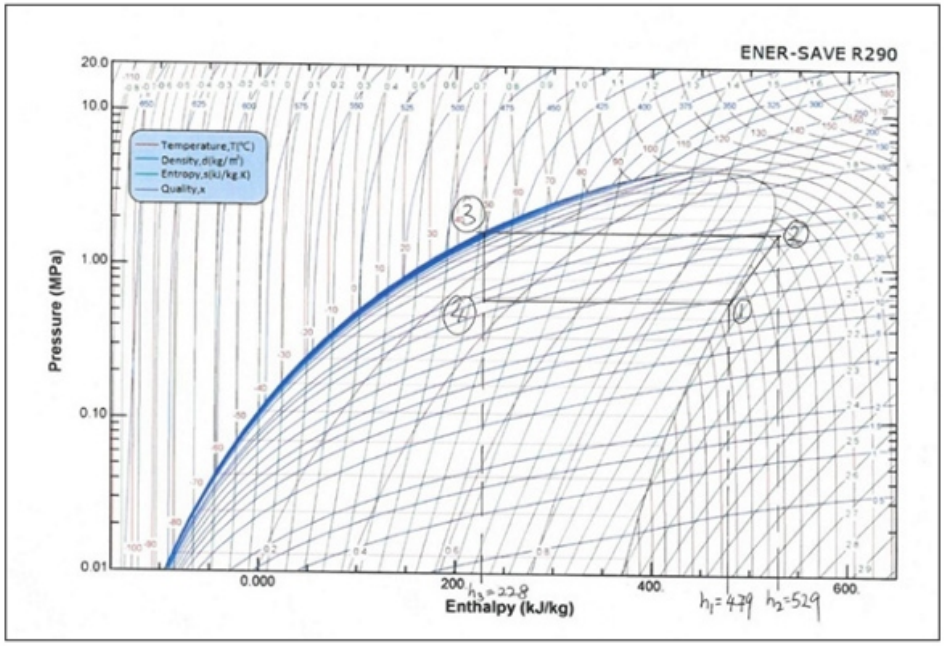

Figure 9. Pressure-enthalpy plotting of R290 air refrigeration system

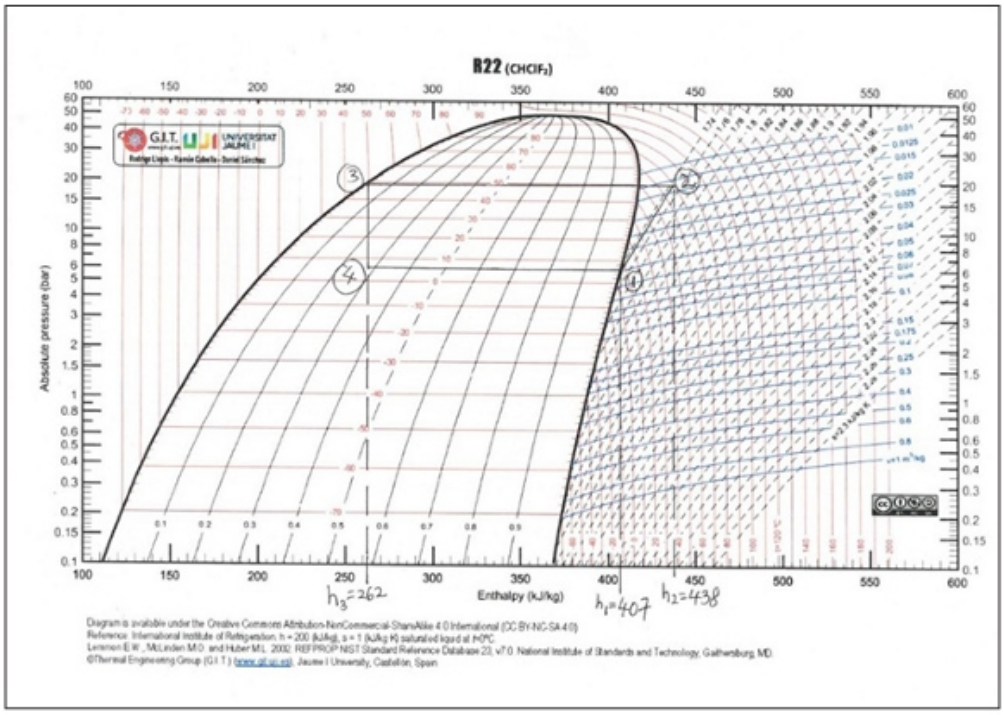

Figure 10. Pressure-enthalpy plotting of the R22 refrigeration system

The mass flow of the refrigerant, mR , can be obtained from Equation 4. The whole process relies on the compressor's external power. Therefore, the work done during the compression cycle is significant in identifying the performance of the refrigeration cycle, as the other states' work was merely the same. Work done during refrigerant compression can be obtained from Equation 5; subsequently, the coefficient of performance, COP, can be calculated from Equation 6. The work done on the compression cycle and refrigeration COP are calculated and shown in Table 6.

Table 6
Work done on compression cycle and refrigeration COP in theory

Refrigerant Type	Work Done During Compression Cycle	COP
R290	482 Watt	5.020
R22	517 Watt	4.677

Apparently, the R290 system draws less power for the compression cycle if compared to the R22 system. Furthermore, the COP of the R290 refrigeration cycle shows a 7.33% increase in the R22 system in the theoretical approach.

Energy Saving Verification and System COP in Practical Case Study

Electrical data collection and observation were conducted concurrently. The practical operating comparison is based on each air conditioner's operating power and cooling performance.

From Table 4, the R290 refrigerant air conditioner consumes instantaneous real at 0.735 kW with a cooling capacity of 0.688 refrigeration tonnage (RT). The specific power value effectively illustrates its efficiency in terms of how much electrical power is used to generate one RT of cooling capacity. The specific power can be derived using Equation 7. In this study, the specific power of the R290 refrigerant air conditioner is calculated to be 1.068 kW/RT, while the specific power of the R22 refrigerant air conditioner is 1.300 kW/ RT. Based on specific power, the R290 refrigerant air conditioner is 17.85% more efficient than the existing R22 refrigerant air conditioner.

From the specific power obtained, the COP in practical operation could be derived from Equation 8. Hence, the COP of an R290 refrigerant air conditioner in practical operation is 3.293, and the COP of an R22 refrigerant air conditioner in practical operation is 2.705. It shows a 21.74% increase in COP after converting to R290 natural refrigerant.

In conjunction with the Malaysian Department of Environment program and based on the SEDA 2016 report, the Co2 equivalent emissions per hour of air conditioner power consumption are calculated by multiplying the total power consumption per hour by Peninsular Malaysia's Co2 emission coefficient rate of 0.639 kg per kWh of electrical usage. Thus, the R290 refrigerant air conditioner would produce 0.509 kg of CO2 equivalent emissions per usage hour (0.735 kW × 1 hr × 0.639 kg/kWh). In comparison, the R22 refrigerant air conditioner would produce 0.617 kg of Co2 equivalent emissions per hour (0.893 kW × 1 hr × 0.639 kg/kWh). The CO2 emissions equivalent produced by the R290 air conditioner are 17.5% lower than those produced by the R22 refrigerant air conditioner. The R290 refrigerant air conditioner is more energy efficient.

Lastly, the direct impact of refrigerants on global warming is determined by multiplying the amount of refrigerant mass charge per air conditioner by the refrigerant's GWP. The direct Co2 equivalent for R290 refrigerant equals 240 grams multiplied by three (R290 refrigerant has a GWP of 3). For R22 refrigerant, the direct CO2 equivalent equals 550 grams multiplied by 1810 (as R22 refrigerant has a GWP of 1810). The release of R290 refrigerant from a 9,000 BTU/hr air conditioner will result in a CO2 equivalent impact of 0.72 kg. Releasing R22 refrigerant from a 9,000 BTU/hr air conditioner will result in a CO2 equivalent impact of 995.50 kg. Therefore, the R290 refrigerant air conditioner is 1,383 times more

environmentally friendly than the R22 refrigerant air conditioner.

CONCLUSION

The hydrocarbon (HC) R290 refrigerant exhibits a lower molecular weight and the highest latent heat of vaporization at its boiling point. It is compatible with both mineral oil and synthetic compressor oils. The lower molecular weight reduces the torsion power required by the compressor, while the higher latent heat of vaporization aids in absorbing more heat within the R290 refrigerant. The compatibility with both compressor oils allows R290 to be effectively converted for use in existing domestic air conditioners. This approach offers an economical solution to address environmental concerns related to transitioning from ozone-depleting and global-warming refrigerants to natural refrigerants. Remarkably, the results of using R290 refrigerant in existing R22 air conditioners indicate a 17.69% reduction in instantaneous power consumption.

From a technical perspective, the hydrocarbon R290 refrigerant enhances the air conditioner's coefficient of performance (COP) by 21.74% in practical terms and by 7.33% in theoretical analysis based on the pressure-enthalpy chart. This increase in COP leads to energy savings through reduced power consumption by the R290 air conditioner. In terms of environmental impact and global warming, adopting the natural refrigerant R290 in domestic air conditioners significantly reduces the impact to 720 grams Co2 equivalent for each R290 system conversion, given its GWP of 3. It starkly contrasts the 995.5 kilograms CO2 equivalent emitted by an R22 system with a GWP of 1810. It equates
to a 1,383 times reduction in CO2 equivalent released into the environment over one when an air conditioner is disposed of in a garbage disposal area.

Safety is paramount when adopting new refrigerants, and we assess the safety aspects of R290. The HC air conditioner's safety compliance, verified through refrigerant mass charge safety verification, and the application of the R290 natural refrigerant air conditioner have been confirmed. The system's flammability is five times lower than the lower flammability limit (LFL) of R290, making it safe for household use and compliant with international standards. However, certain safety precautions are essential to educate users and installers, such as avoiding installation of the R290 system near ignition sources. Electrical components need to be switched to solid-state components; for instance, glasstype fuses are recommended to be replaced with ceramic types on the printed circuit board. Overcoming flammability concerns involves adopting good practices and designs.

Furthermore, to mitigate carbon emissions through the use of HC in domestic air conditioners,

refrigerants like synthetic R22 need to be recovered into empty cylinders for recycling, reclamation, and reuse. According to Table 4, each R290 conversion from an existing R22 system (9000 BTU/hr) can directly reduce CO2 equivalent impact by 994.78 kg due to the refrigerant's global warming potential, making it 1,383 times greener. projected reduction in carbon dioxide from electricity savings is estimated at about 17.5%, potentially leading to a reduction of up to 0.108 kg of CO2 emissions per hour of usage for each air conditioner.

Considering the scenario of converting 200,000 units of R22 air conditioners to R290 natural refrigerant instead of replacing them with other high global warming type air conditioners, it could result in a reduction of up to 198.956 million kg of CO2 equivalent from refrigerant direct impact and 21,600 kg of CO2 reduction per hour of electricity usage. Environmental sustainability is a critical factor in evaluating refrigerants, and our study presents compelling evidence in favour of hydrocarbon R290. By adopting natural refrigerants, we have the potential to mitigate climate change by reducing the usage of high global warming substances found in traditional synthetic refrigerants. Embracing this change on a larger scale could substantially impact the environment and help address challenges of global warming.

ACKNOWLEDGEMENT

The author thanks Ener-Save Green Air Conditioner Sdn Bhd for providing facilities, tools and equipment during this research.

REFERENCES

ASHRAE. (2022). ASHRAE refrigerant designations. ASHRAE. https://www.ashrae.org/technical-resources/ standards-and-guidelines/ashrae-refrigerant-designations

Cengel, Y., & Boles, M. (2015). Thermodynamics an engineering approach (8th ed.). McGraw-Hill Education.

EPA. (n.d.). Global Greenhouse gases emissions data. United States Environmental Protection Agency. https:// www.epa.gov/ghgemissions/global-greenhouse-gas-emissions-data

European Commission. (2022). Climate action. European Commission. https://climate.ec.europa.eu/eu-action/ fluorinated-greenhouse-gases/overview_en

Khurmi, R. S., & Gupta, J. K. (2008). A textbook of refrigeration and air conditioning. (4th ed.). S. Chand Publishing.

Ministry of Natural Resources and Environmental Sustainability. https://www.doe.gov.my/en/2021/10/26/ malaysia-committed-to-the-protection-of-the-ozone-layer-

-and-the-earths-climate-through-the-ratification of-the-kigali-amendment-under-the-montreal-protocol/

MS2678 Working Group. (2017). Malaysian Standard MS 2678:2017, Flammable refrigerant system – Code of practice. Department of Standards Malaysia.

Ng, F. (2021). Ener-save hydrocarbon refrigerants training manual. Ener-Save Sdn Bhd.

Rusyanto, P. (2021). Environmental impact of HFO refrigerants & alternatives for the future. Open Access Government Team. https://www.openaccessgovernment.org/hfo-refrigerants/112698/

SEDA Malaysia. (2019). CO2 Avoidance. Sustainable Energy Development Authority (SEDA) Malaysia. https://www.seda.gov.my/statistics-monitoring/co2-avoidance/

United Nations Climate Change. (2016). 28th meeting of the parties to the Montreal protocol. United Climate Change. https://unfccc.int/news/28th-meeting-parties-montreal-protocol?gclid=EAIaIQobChMIpe6y2qaw_wIVx6GWCh1abgmlEAAYASAAEgJFMPD_BwE

Instructions for Authors

Essentials for Publishing in this Journal

1 Submitted articles should not have been previously published or be currently under consideration for publication elsewhere.

2 Conference papers may only be submitted if the paper has been completely re-written (taken to mean more than 50%) and the author has cleared any necessary permission with the copyright owner if it has been previously copyrighted.

3 All our articles are refereed through a double-blind process.

4 All authors must declare they have read and agreed to the content of the submitted article and must sign a declaration correspond to the originality of the article.

Submission Process

All articles for this journal must be submitted using our online submissions system. http://enrichedpub.com/ . Please use the Submit Your Article link in the Author Service area.

Manuscript Guidelines

The instructions to authors about the article preparation for publication in the Manuscripts are submitted online, through the e-Ur (Electronic editing) system, developed by **Enriched Publications Pvt. Ltd**. The article should contain the abstract with keywords, introduction, body, conclusion, references and the summary in English language (without heading and subheading enumeration). The article length should not exceed 16 pages of A4 paper format.

Title

The title should be informative. It is in both Journal's and author's best interest to use terms suitable. For indexing and word search. If there are no such terms in the title, the author is strongly advised to add a subtitle. The title should be given in English as well. The titles precede the abstract and the summary in an appropriate language.

Letterhead Title

The letterhead title is given at a top of each page for easier identification of article copies in an Electronic form in particular. It contains the author's surname and first name initial .article title, journal title and collation (year, volume, and issue, first and last page). The journal and article titles can be given in a shortened form.

Author's Name

Full name(s) of author(s) should be used. It is advisable to give the middle initial. Names are given in their original form.

Contact Details

The postal address or the e-mail address of the author (usually of the first one if there are more Authors) is given in the footnote at the bottom of the first page.

Type of Articles

Classification of articles is a duty of the editorial staff and is of special importance. Referees and the members of the editorial staff, or section editors, can propose a category, but the editor-in-chief has the sole responsibility for their classification. Journal articles are classified as follows:

Scientific articles:

1. Original scientific paper (giving the previously unpublished results of the author's own research based on management methods).

2. Survey paper (giving an original, detailed and critical view of a research problem or an area to which the author has made a contribution visible through his self-citation);

3. Short or preliminary communication (original management paper of full format but of a smaller extent or of a preliminary character);

4. Scientific critique or forum (discussion on a particular scientific topic, based exclusively on management argumentation) and commentaries. Exceptionally, in particular areas, a scientific paper in the Journal can be in a form of a monograph or a critical edition of scientific data (historical, archival, lexicographic, bibliographic, data survey, etc.) which were unknown or hardly accessible for scientific research.

Professional articles:

1. Professional paper (contribution offering experience useful for improvement of professional practice but not necessarily based on scientific methods);
2. Informative contribution (editorial, commentary, etc.);
3. Review (of a book, software, case study, scientific event, etc.)

Language

The article should be in English. The grammar and style of the article should be of good quality. The systematized text should be without abbreviations (except standard ones). All measurements must be in SI units. The sequence of formulae is denoted in Arabic numerals in parentheses on the right-hand side.

Abstract and Summary

An abstract is a concise informative presentation of the article content for fast and accurate Evaluation of its relevance. It is both in the Editorial Office's and the author's best interest for an abstract to contain terms often used for indexing and article search. The abstract describes the purpose of the study and the methods, outlines the findings and state the conclusions. A 100- to 250-Word abstract should be placed between the title and the keywords with the body text to follow. Besides an abstract are advised to have a summary in English, at the end of the article, after the Reference list. The summary should be structured and long up to 1/10 of the article length (it is more extensive than the abstract).

Keywords

Keywords are terms or phrases showing adequately the article content for indexing and search purposes. They should be allocated heaving in mind widely accepted international sources (index, dictionary or thesaurus), such as the Web of Science keyword list for science in general. The higher their usage frequency is the better. Up to 10 keywords immediately follow the abstract and the summary, in respective languages.

Acknowledgements

The name and the number of the project or programmed within which the article was realized is given in a separate note at the bottom of the first page together with the name of the institution which financially supported the project or programmed.

Tables and Illustrations

All the captions should be in the original language as well as in English, together with the texts in illustrations if possible. Tables are typed in the same style as the text and are denoted by numerals at the top. Photographs and drawings, placed appropriately in the text, should be clear, precise and suitable for reproduction. Drawings should be created in Word or Corel.

Citation in the Text

Citation in the text must be uniform. When citing references in the text, use the reference number set in square brackets from the Reference list at the end of the article.

Footnotes

Footnotes are given at the bottom of the page with the text they refer to. They can contain less relevant details, additional explanations or used sources (e.g. scientific material, manuals). They cannot replace the cited literature.
The article should be accompanied with a cover letter with the information about the author(s): surname, middle initial, first name, and citizen personal number, rank, title, e-mail address, and affiliation address, home address including municipality, phone number in the office and at home (or a mobile phone number). The cover letter should state the type of the article and tell which illustrations are original and which are not.